Late Quaternary climate variability at Mfabeni peatland, eastern South Africa

Charlotte Miller[1*], Jemma Finch[2], Trevor Hill[2], Francien Peterse[3], Marc Humphries[4], Matthias Zabel[1], Enno Schefuß[1]

[1]MARUM - Center for Marine Environmental Sciences, University of Bremen, Bremen, Germany
[2]School of Agricultural, Earth and Environmental Sciences, University of KwaZulu-Natal, Pietermaritzburg, South Africa
[3]Department of Earth Sciences, Utrecht University, Netherlands
[4]Molecular Sciences Institute, School of Chemistry, University of the Witwatersrand, Johannesburg, South Africa
*Correspondence email: lottiemiller2@gmail.com

Abstract

The scarcity of continuous, terrestrial, palaeoenvironmental records in eastern South Africa leaves the evolution of late Quaternary climate and its driving mechanisms uncertain. Here we use a ~7-m long core from Mfabeni peatland (KwaZulu-Natal, South Africa) to reconstruct climate variability for the last 32 thousand years (cal ka BP). We infer past vegetation and hydrological variability using stable carbon ($\delta^{13}C_{wax}$) and hydrogen isotopes (δD_{wax}) of plant-wax *n*-alkanes and use P_{aq} to reconstruct water table changes. Our results indicate that late Quaternary climate in eastern South Africa did not respond directly to orbital forcing nor to changes in sea surface temperatures (SSTs) in the western Indian Ocean. We attribute the arid conditions evidenced at Mfabeni during the Last Glacial Maximum (LGM) to low SSTs and an equatorward displacement of: i) the southern hemisphere westerlies, ii) the subtropical high-pressure cell and iii) the South Indian Ocean Convergence Zone (SIOCZ), due to increased Antarctic sea ice extent. The northerly location of the high-pressure cell and the SIOCZ inhibited moisture advection inland and pushed the rain-bearing cloud band north of Mfabeni, respectively. The increased humidity at Mfabeni between 19–14 cal kyr BP likely resulted from decreased Antarctic sea ice, which led to a southward retreat of the westerlies, the high-pressure cell and the SIOCZ. Between 14–5 cal kyr BP, when the westerlies, the high-pressure cell and the SIOCZ were in their southernmost position, local insolation became the dominant control, leading to stronger atmospheric convection and an enhanced tropical easterly monsoon. Generally drier conditions persisted during the past *c*. 5 cal ka BP, probably resulting from an equatorward return of the westerlies, the high-pressure cell and the SIOCZ. Higher SSTs and heightened ENSO activity may have played a role in enhancing climatic variability during the past *c*. 5 cal ka BP. Our findings highlight the

influence of the latitudinal position of the westerlies, the high-pressure cell and SIOCZ in driving climatological and environmental changes in eastern South Africa.

Key words: Mfabeni; eastern South Africa; *n*-alkanes; hydrogen isotopes; carbon isotopes; southern hemisphere westerlies; tropical easterlies

1. Introduction

Eastern South Africa is an important region for scientific focus, specifically for furthering our understanding of regional and global climate dynamics. The region is particularly dynamic and sensitive to long-term climate change as it lies within a climatic transition zone, where it is strongly influenced by both temperate (southern westerlies) and tropical (tropical easterlies) climate systems. In eastern South Africa, modelled precipitation reductions and projected regional warming (3–6°C by 2099), threaten the stability of current ecosystems in a region populated by communities already economically vulnerable to the effects of climate change (IPCC, 2013). Past climate and environmental reconstruction and the determination of climate driving mechanisms will provide valuable information for assessing future climate and environmental trends in the region.

Changes in vegetation, precipitation and temperature from the beginning of the Last Glacial Maximum (LGM; *c*. 26.5 ka; Clark et al., 2009) to present-day, are poorly constrained in eastern South Africa. Whether this region was characterized by aridity or increased humidity during the last glacial period remains unclear. Proxy data show spatial complexity (e.g. Baker et al., 2016; Chase et al., 2017; Chevalier and Chase, 2015 & 2016, Dupont et al., 2011; Schefuß et al., 2011; Scott et al., 2012; Scott, 2016; Schmidt et al., 2014; Simon et al., 2015), and modelled LGM (26.5–19 ka; Clark et al., 2009) precipitation for the region are highly variable and often do not even agree on the sign of precipitation change. For example, the PMIP3 model ensemble mean suggests increased LGM precipitation in the east of South Africa with dry conditions towards the north (compared to the present day; Braconnot et al., 2007; Chevalier et al., 2017). Conversely, the NCAR CCSM3 model indicates drier than present conditions in the centre of South Africa and along the eastern coast (Otto-Bliesner et al., 2006). These contrasting simulations for the last glacial period highlight the difficulty in simulating past precipitation in South Africa, with a lack of a comprehensive understanding regarding the relevant climate processes involved (Stone, 2014).

The mechanisms driving Quaternary climate variability in South Africa are complex and spatially heterogeneous. For example, hydroclimate may be paced by austral summer insolation fluctuations, resulting from changes in the Earth’s orbital precession on 23–19 ka timescales. Strong summer insolation (during precession maxima) causes stronger atmospheric convection and an increase in the land/ocean temperature contrast, which results in higher moisture transport by the tropical easterlies and higher precipitation in eastern South Africa (e.g. Simon et al., 2015; Chevalier and Chase, 2015). Climate may also be influenced by high-latitude forcing related to changes in the Earth's orbital obliquity and eccentricity on longer, i.e. glacial-interglacial timescales, which may result in the latitudinal contraction and expansion of the climatic belts (e.g. Dupont, 2011). The model of Nicholson and Flohn (1980) suggests an equatorward displacement of the tropical rainbelt (Nicholson, 2008) during the last glacial period, although proxy data from South Africa provide no conclusive support for this scenario. In addition, during glacial periods, the Walker Circulation may have been weaker with its ascending limb further to the east, over the Indian Ocean (e.g. DiNezio et al., 2018). This possibly resulted in an eastward displacement of the cloud band (SIOCZ) and thus a drier summer rainfall zone (SRZ; Tyson, 1999). Furthermore, changes in the latitudinal position of the southern hemisphere westerlies (as a response to fluctuations in Antarctic sea ice extent) have been invoked to influence climate in South Africa (Chase and Meadows, 2007; Chevalier and Chase, 2015; Chase et al., 2017). The western South African region has received most focus regarding the southern hemisphere westerly influence in controlling climate variability (e.g. Stuut et al., 2004; van Zinderen Bakker, 1976). Some studies also suggest possible mechanistic links between SSTs in the Agulhas Current and the Indian Ocean and rainfall variability in South Africa, with high SSTs linked to increasing South African summer precipitation (e.g. Baker et al., 2017; Chevalier and Chase, 2015; Dupont, 2011; Dupont et al., 2011; Reason and Mulenga, 1999). Climate forcing experiments also indicate that changes in greenhouse gas concentrations may have driven eastern South African rainfall changes, increasing precipitation between 17–11 kyr (Otto-Bliesner et al., 2014).

The spatially heterogeneous nature of climate variability in South Africa from the last glacial period to the present-day, and the multiple possible climate drivers render the region an important focus for palaeoclimate research. Two important questions remain: i) what was the climate like in eastern South Africa during the last glacial period? and, ii) what were the causes for the climate variability? These questions are difficult to answer with the majority of long, continuous, terrestrial records situated further north, within the range of the modern tropical rainbelt (e.g. Barker et al., 2007; Tierney et al., 2008), making it hard to assess the long-term climate drivers in the south, in particular in eastern South Africa. In this area, terrestrial sediment archives suitable for palaeoenvironmental reconstruction are scarce, in particular those extending to the LGM. Marine and speleothem archives have hitherto mostly formed the basis of Quaternary climate research in this region (e.g. Dupont et al., 2011; Holmgren et al., 2003). Here we provide stable carbon (δ^{13}C) and hydrogen (δD) isotope records of terrestrial plant-waxes (long-chained *n*-alkanes) from Mfabeni peatland, one of the longest continuous terrestrial archives from South Africa. Our vegetation and hydroclimate reconstructions are compared with a previous biomarker-palaeoclimate study from Mfabeni (Baker et al., 2014, 2016 & 2017). We more than double the temporal resolution of the previous plant-wax δ^{13}C record from

Baker et al. (2017), from *c*. 1200 to *c*. 500 years, revealing important and previously undocumented environmental variability.

2. Regional setting

The mid-latitude westerlies, in association with the subtropical high (and low) pressure cells and the SIOCZ, play critical roles in determining climatic conditions across the whole South African continent (Fig. 1; Dyson and van Heerden, 2002; Macron et al., 2014; Munday and Washington, 2017). During austral winter, an anti-clockwise rotating subtropical high-pressure cell is located over southern Africa, which drives large-scale subsidence and suppresses rainfall (Fig. 1b). This high-pressure cell creates a blocking effect over the continent, which stops moisture advection inland over the majority of South Africa during winter (Dedekind et al., 2016), except for in the winter rainfall zone (WRZ), where the westerlies bring rainfall. During summer, the high-pressure cell shifts to the south, and the Angola and Kalahari low pressure cells dominate the continent, enabling monsoonal systems (tropical easterlies) to penetrate southern Africa, bringing rainfall to the summer rainfall zone (SRZ; Fig. 1a; Tyson and Preston-Whyte, 2000; Munday and Washington, 2017). The dominant rain-producing mechanism in the SRZ during the summer are tropical temperature troughs (TTTs), which are embedded within the SIOCZ and form a northwest-southeast orientated cloud band, extending over the continent into the southwest Indian Ocean (Fig. 1a; Todd and Washington 1999; Tyson and Preston-Whyte, 2000). TTTs form from interactions between tropical convection and mid-latitude perturbations, which result in heavy precipitation events (Tyson, 1986; Macron et al., 2014; Chase et al., 2017). A combination of strong easterly flux from the Indian Ocean and low pressure over the continent during the summer results in the development of TTTs (Fig. 1a; Cook, 2000; Macron et al., 2014; Rácz and Smith, 1999; Todd and Washington 1999).

South Africa can be divided into several climate zones: the SRZ lies in the north and east where 66 % of the mean annual precipitation falls between October and March (Fig. 1a; Chase and Meadows, 2007). Based on late Quaternary precipitation reconstructions, further subdivisions of the SRZ (northern SRZ, central/eastern SRZ) have been suggested by Chevalier and Chase (2015). In the extreme south and west of South Africa lies the WRZ (Fig. 1a), where 66 % of the mean annual precipitation falls between April and September (Chase and Meadows, 2007). This rainfall is associated with temperate frontal systems related to the southern hemisphere westerlies (Fig. 1b; Mason and Jury, 1997; Tyson, 1986; Tyson and Preston-Whyte, 2000). In between the SRZ and WRZ lies the year-round rainfall zone (YRZ) which receives precipitation both in summer and winter seasons (Fig. 1a; Chase and Meadows, 2007). This zone comprises much of the southern Cape of South Africa and is highly heterogeneous in terms of precipitation seasonality and amount, spanning some of the wettest (e.g. along the south coast), and driest (e.g. Namib Desert) regions in South Africa.

Mfabeni peatland is located within the SRZ, on the coastal plain of northern KwaZulu-Natal (28°09′8.1″S; 32°31′9.4″E; 9 m above sea level; Fig. 1; Fig. 2). The dominating subtropical high-pressure cell across the majority of South Africa during the austral winter months leads to mild and dry winter conditions at Mfabeni. Occasional rainfall during the winter months at Mfabeni is associated with the passage of cold fronts, which develop in the western Atlantic and move across southern Africa (Fig. 1b; Grab and Simpson, 2000). These cold fronts trigger rainout of atmospheric moisture, which is sourced from the Indian Ocean and Agulhas region (Gimeno et al., 2010). When the subtropical high-pressure cell has moved south during the austral summer, the tropical easterlies dominate, TTTs form and conditions at Mfabeni are hot and humid. The average annual rainfall amount between 2010 and 2018 at Mfabeni in the winter months (June–August) was measured at 134 mm compared to 426 mm during the summer months (December–February), meaning the majority of rainfall (76 %) falls during the summer months (data from World Weather Online). A northeast–southwest precipitation gradient is present across the peatbog, with 1200 mm year^{-1} of precipitation in the east decreasing to 900 mm year^{-1} westwards towards Lake St. Lucia (Fig. 1; Fig. 2; Taylor et al., 2006). The main source of water to Mfabeni is precipitation, predominantly provided by the tropical easterlies and TTTs, sourced from the Indian Ocean and Agulhas Current region (Fig. 1; Tyson, 1999; Gimeno et al., 2010). Mean summer temperatures (November to March) surpass 21 °C. The wind regime is characterised by moderate northeasterly winds during the summer and more intense southwesterly winds during winter.

Mfabeni is one of the oldest, continuously growing peatlands in South Africa (Grundling et al., 2013). It lies within a topographical inter-dunal depression between the Indian Ocean to the east and Lake St. Lucia to the west (Fig. 2; Grundling et al., 2013). Towards the ocean, it is bordered by an 80–100 m high vegetated dune barrier, and to the west by the 15–70 m high Embomveni sand dune ridge (Fig. 2). Over the last 44 ka, the mire accumulated *c*. 11 m of peat, deposited on top of a basal clay layer (Grundling et al., 2015). This clay layer was crucial in the formation and development of the mire, limiting water loss during low sea level stands (Grundling et al., 2013). Mfabeni is bound to the north and south by beach ridges isolating it from Lake Bhangazi and Lake St. Lucia, respectively (Fig. 2; Grundling et al., 2013). When lake levels in Lake Bhangazi are high, minor water exchange between Mfabeni and Bhangazi occurs, but there are no fluvial inputs to either system. Surface drainage occurs southwards towards Lake St Lucia (Fig. 2). The peatland receives groundwater via the swamp forest and the western dunes. This groundwater, which is important in keeping the mire wet during the dry season, discharges towards the center of the peatland and then flows within a sub-surface layer towards the east (Grundling et al., 2015). In the northern and eastern part of the peatland, the vegetation is sedge and reed fen (comprising of sedges and grasses). In the western and southern parts of Mfabeni is swamp forest (Venter, 2003).

The modern water balance at Mfabeni is dominated by the interplay between evapotranspiration (ET; 1035 mm) and precipitation (1053 mm). Groundwater inflow (14 mm) and stream outflow (9 mm) have a minor contribution to the modern water balance (all measured between May 2008 and April 2009; Grundling et al., 2015). Changes in regional climate have much potential to influence the fine balance between ET and precipitation. For example, ET is suppressed when cloud cover is increased during the summer months and increased during times of higher wind speed (Grundling et al., 2015). ET is higher in the swamp forest than in the sedge and reed fen, therefore a change in vegetation composition also has the potential to impact ET rates. The depositional setting of the Mfabeni peatland provides a unique opportunity to reconstruct past eastern South African climate variability at centennial-scale resolution from the Late Pleistocene to the present day.

3. Methodological background

To reconstruct past vegetation and hydroclimate we use the distribution, and the carbon and hydrogen isotopic composition, of long chain *n*-alkanes derived from plant-waxes.

3.1 Distributions of plant-waxes

To obtain information on water table variations, we quantify the relative contribution of plant-waxes derived from submerged and floating macrophytes relative to that of emergent and terrestrial plants (P_{aq}). Odd-numbered *n*-alkanes (C_{25}–C_{35}) are derived from the epicuticular wax coating of terrestrial higher plants (Eglinton and Hamilton, 1967). Conversely, aquatic plant-waxes (of submerged macrophyte origin) are dominated by mid-chain *n*-alkanes (typically C_{23} and C_{25}; e.g. Baker et al., 2016; Ficken et al., 2002). Thus we quantify P_{aq} using Equation 1 (Ficken et al., 2000).

$$P_{aq} = (C_{23} + C_{25})/(C_{23} + C_{25} + C_{29} + C_{31}) \quad \text{Eq. 1}$$

with C_x the amount of each homologue.

To assess *n*-alkane degradation we used the carbon preference index (CPI; Bray and Evans, 1961). The CPI reflects the molecular distribution of odd-to-even *n*-alkanes, within a certain carbon number range (here, *n*-C_{26} to *n*-C_{34}; Equation 2). High CPI values indicate a higher contribution of odd-numbered *n*-alkanes (relative to even), indicating the *n*-alkanes are derived from higher terrestrial plants. Low CPI values indicate either low contribution from terrestrial higher plants or high organic matter degradation (Eglinton and Hamilton, 1967).

$$CPI_{27\text{-}33} = 0.5 * (\Sigma C_{odd27\text{-}33}/\Sigma C_{even26\text{-}32} + \Sigma C_{odd27\text{-}33}/\Sigma C_{even28\text{-}34}) \quad \text{Eq. 2}$$

with C_x the amount of each homologue.

3.2 Carbon and hydrogen isotopes of terrestrial plant-waxes

To reconstruct vegetation changes, we use the carbon isotopic composition of terrestrial plant-waxes ($\delta^{13}C_{wax}$). On late Quaternary timescales, the primary factor determining the amplitude of fractionation between the $\delta^{13}C$ of atmospheric CO_2 ($\delta^{13}C_{atm}$) and the carbon isotopic composition of the plant ($\delta^{13}C_{plant}$) is the plant carbon fixation pathway (C_3/C_4/CAM; e.g. Diefendorf and Freimuth, 2017). On these timescales, changes in the $\delta^{13}C_{atm}$ are too small to significantly influence $\delta^{13}C_{wax}$ (Tipple et al., 2010). Shrubs and trees use the C_3 photosynthetic pathway and show the largest fractionation. Grasses utilize either the C_3 or the C_4 pathway, with C_4 plants having the smallest net fractionation (Collister et al., 1994). The differences in carbon isotope fractionation during carbon uptake leads to different $\delta^{13}C_{wax}$ signatures, and allows the determination of past vegetation types: *n*-alkane $\delta^{13}C$ values of C_3 plants are *c*. -36‰ VPDB (Vienna Pee Dee Belemnite) and *c*. -20‰ VPDB for C_4 plants (e.g. Diefendorf and Freimuth, 2017).

The hydrogen isotope composition of plant-waxes (δD_{wax}) reflects the isotopic composition of the water used during lipid biosynthesis (Sachse et al., 2012), rendering it a valuable tool for reconstructing past hydrological conditions (e.g. Collins et al., 2013; Schefuß et al., 2005). δD_{wax} is influenced by three main factors: i) the isotopic composition of precipitation; ii) enrichment of soil and leaf water due to ET; and iii) differences in the apparent isotopic fractionation between source water and plant-waxes due to differences in vegetation type. The importance of each factor varies by study site and with time. The detailed interpretation of the Mfabeni $\delta^{13}C_{wax}$ and δD_{wax} is discussed in section 6.1.

4. Methods: compound specific C and H isotope analyses

Core MF4-12 (6.96 m recovery, 8.77 m penetration) was recovered from the centre of Mfabeni peatland during January 2012 using a vibrocoring device (Fig. 2). The chronology of the core is established by 24 ^{14}C AMS (accelerator mass spectrometry) dates from bulk peat (Fig. 3, S1). The chronology is extended from that published in Humphries et al. (2017) and the age model is made using Bacon 2.2 program (Blaauw and Christen, 2011). Radiocarbon ages were calibrated using the southern hemisphere calibration curve, ShCal13 (Hogg et al., 2016) and the post-bomb southern hemisphere curve, zone 1–2, for the uppermost modern dates (Hua et al., 2016).

Freeze-dried, bulk peat samples were ground and homogenized using a pestle and mortar and lipids were extracted from *c*. 2 g of peat using a DIONEX Accelerated Solvent Extractor (ASE 200) at 100 °C and at 1000 psi for 5 minutes (repeated 3 times) using a dichloromethane (DCM):methanol (MeOH) (9:1, v/v) mixture. Prior to extraction, squalane was added as an internal standard. Copper turnings were used to remove elemental sulfur from the total lipid extract (TLE). To remove water, the TLE was passed over a Na_2SO_4 column (eluting with hexane). Subsequent to saponification (by adding 6 % KOH in MeOH) and extraction (with hexane), the neutral fractions were split into a further three fractions: hydrocarbon, ketone, and polar, by silica gel column chromatography (mesh size 60 µm) and elution with hexane, DCM and DCM:MeOH (1:1), respectively. By eluting the hydrocarbon fractions with hexane over $AgNO_3$-impregnated silica columns we obtained the saturated hydrocarbon fractions. The saturated hydrocarbon fractions were measured using a Thermo Fischer Scientific Focus gas-chromatograph (GC) with flame-ionization-detection (FID) equipped with a Restek Rxi 5ms column (30 m x 0.25 mm x 0.25 µm), in order to determine the concentrations of long-chain *n*-alkanes. The GC oven temperature was set at 60 °C, held for 2 minutes, increased at 20 °C/minute to 150 °C and then at 4 °C/minute to 320 °C and held for 11 minutes. The split/splitless inlet temperature was 260 °C. To estimate the sample concentrations needed for isotope analyses, samples were compared with an external standard that was run every 5 samples, which contained *n*-alkanes (C_{19}–C_{34}) at a concentration of 10 ng/µl. A quantification uncertainty of <5% was yielded through replicate analyses of the external standard.

The $\delta^{13}C$ values of the long-chain *n*-alkanes were measured using a Thermo Trace GC Ultra equipped with an Agilent DB-5 column (30m x 0.25mm x 0.25µm) coupled to a Finnigan MAT 252 isotope ratio mass spectrometer (IR-MS) via a combustion interface operated at 1000 °C. The GC temperature was programmed from 120 °C (hold time 3 min), followed by heating at 5 °C/minute to 320 °C (hold time 15 minutes). The external CO_2 reference gas was used to calibrate the $\delta^{13}C$ values and they are reported in ‰ VPDB. Samples were analysed in duplicate when *n*-alkane concentrations were adequate for multiple runs. The internal standard (squalane, $\delta^{13}C$= -19.9‰), yielded an accuracy of 0.6‰ and a precision of 0.2‰ (n=37). The external standard mixture was analysed every 6 runs. The long-term precision and accuracy of the external *n*-alkane standard was 0.2 and 0.15‰, respectively. For $\delta^{13}C$ the average precision of the *n*-C_{29} and *n*-C_{31} alkane in replicates was 0.2‰ and 0.1‰ (n=22), respectively.

The δD compositions of long-chain *n*-alkanes were measured using a Thermo Trace GC coupled via a pyrolysis reactor (operated at 1420 °C) to a Thermo Fisher MAT 253 IR-MS. The GC column and temperature program was similar to that used for the $\delta^{13}C$ analysis. The external H_2 reference gas was used to calibrate the δD values and they are reported in ‰ VSMOW. The H^{3+} factor was monitored daily and fluctuated around 5.2 ppm nA^{-1} during analyses. After every sixth measurement, an *n*-alkane standard of 16 externally calibrated alkanes was measured. The long-term precision and accuracy of the external *n*-alkane standard was 2.7 and 2‰, respectively. Samples were analysed in duplicate when *n*-alkane concentrations were adequate for multiple runs. The internal standard (squalane, δD=

-180‰; ±2), yielded an accuracy of 0.9‰ and a precision of 1.9‰ (n=36). For δD the average precision in replicates was 1‰ for both *n*-C_{29} and *n*-C_{31} alkanes (n=52).

The last glacial period Mfabani δD_{wax} values were corrected to account for the effect of changes in global ice volume (Collins et al., 2013; Schefuß et al., 2005). For this, the benthic foraminifera-based oxygen isotope curve (Waelbroeck et al., 2002) was interpolated to each sample age and then converted to δD values using the global meteoric water line (Craig, 1961).

5. Results

This study focusses on the last 32 cal ka BP (*c*. 590 cm). The average temporal resolution between the 62 samples analysed for δ^{13}C and δD is *c*. 500 years. From 590 to 70 cm (*c*. 32–2 cal kyr BP) the core is very dark brown in colour containing peat with humus, fine detritus and silt. From 70 cm to core top, the sediments are similar in colour to the peat below and contain fibrous peat with humus and herbaceous fine detritus (Humphries et al., 2017). Between 457 and 358 cm (*c*. 23–14 cal kyr BP; comprising the LGM) mean grain sizes average at 110 μm, with smaller diameters averaging at 50 μm between 298 and core top (*c*. 11 cal kyr BP–present, Holocene; Fig. 4g). The lithology of core MF4-12 does not exactly match with that observed from core SL6 (Baker et al., 2014; 2016; 2017), although sandy peat is observed during the LGM at both locations. This result is not surprising as multiple cores taken in transects across the bog indicate peat heterogeneity (Grundling et al., 2013).

Long chain *n*-alkane CPI values are generally around 6 (ranging from 2–13), indicating good *n*-alkane preservation. The two samples with CPI values of 2, potentially containing more degraded *n*-alkanes, are highlighted in red (Fig. 4b & c; Fig. 5b & c; Fig. 6f & g). However, the in- or exclusion of these samples does not affect the observed pattern of changes and we thus consider the record to be suitable for palaeoclimate reconstruction. The samples contain *n*-alkanes with carbon chain lengths ranging from C_{17}–C_{35}, with C_{29} and C_{31} generally having the highest abundance. The high abundances of C_{29} and C_{31} enabled reliable isotopic analyses. The relationship between the δD and δ^{13}C of the C_{29} and C_{31} *n*-alkanes is strong, with R^2 values of 0.8 and 0.9, respectively. Consequently, for the $\delta^{13}C_{wax}$ and δD_{wax}, we use the amount-weighted mean of the C_{29} and C_{31} *n*-alkanes.

The $\delta^{13}C_{wax}$ values range from -29‰ to -21‰ (Fig. 4b). The ice volume δD correction decreases the glacial Mfabeni δD_{wax} values by <8 ‰ (Fig. 4c). The ice-corrected δD_{wax} values of the *n*-C_{29} and *n*-C_{31} alkanes range from -181‰ to -128‰ (Fig. 4c). P_{aq} values range from 0.02–0.7, averaging at 0.2 (Fig. 4f).

During the LGM, $\delta^{13}C_{wax}$ and δD_{wax} values are relatively high averaging at -23‰ and *c*. -136‰, respectively (Fig. 4b & c) and P_{aq} values are low (*c*. 0.24; Fig. 4f). At *c*. 19 cal ka BP a 4‰ negative shift in $\delta^{13}C_{wax}$ values occurs (Fig. 4b). This negative shift in $\delta^{13}C_{wax}$ is concurrent with a gradual shift to lower δD_{wax} values (Fig. 4c) and an increase in P_{aq} values (Fig. 4f). Between 14 and 5 cal kyr BP, $\delta^{13}C_{wax}$ values are relatively stable and average at -28‰ (Fig. 4b). δD_{wax} values become gradually lower during this period reaching -173‰ at 7.5 cal ka BP. At 5 cal ka BP, δD_{wax} values shift towards more positive values by 16‰ (Fig. 4c). Relatively high P_{aq} values occur between 14–5 cal kyr BP (Fig. 4f). After *c*. 5 cal ka BP several high amplitude millennial-scale fluctuations in both $\delta^{13}C_{wax}$ and δD_{wax} values are evident. These fluctuations interrupt a trend where the isotope values of both $\delta^{13}C_{wax}$ and δD_{wax} gradually increase towards present day. A pronounced shift to higher $\delta^{13}C_{wax}$ and δD_{wax} values occurs at 2.8 cal ka BP. From *c*. 900 cal yr BP, $\delta^{13}C_{wax}$ and δD_{wax} values become higher reaching core top values of -21 and -128‰, respectively (Fig. 4b & c). Generally high, but variable and rapidly fluctuating P_{aq} values are evident between *c*. 5–0 cal kyr BP. P_{aq} values decrease substantially after 1.3 cal ka BP from 0.6 to a core top value of *c*. 0 (Fig. 4f).

6. Discussion

6.1 Interpretation of the proxy signals

The relatively high CPI_{27-33} values indicate that the long-chain *n*-alkanes within the peat are derived from terrestrial higher plants and are relatively non-degraded. The long-chain *n*-alkanes are likely sourced directly from the local vegetation surrounding the coring location. It is possible that during times of stronger wind strength (i.e. during the LGM; Humphries et al., 2017) increased aeolian transport resulted in a higher biomarker contribution from more distal sources (i.e. the surrounding dune vegetation). Good preservation of *n*-alkanes in Mfabeni peat was also observed in nearby core SL6, but this was based on a CPI calculated using *n*-C_{21-31} (Baker et al., 2016). No relationship exists between the CPI and P_{aq} (R^2 = 0.11), which suggests that CPI variations at the location of core MF4-12 are not related to changes in organic matter preservation due to water table level variations.

The main source of carbon for terrestrial higher plants (the source of the C_{29} and C_{31} *n*-alkanes) is atmospheric CO_2, whereas aquatics also assimilate dissolved carbon, complicating the interpretation of their carbon isotope signal. We thus focus solely on C_{29} and C_{31} *n*-alkanes that are predominantly derived from terrestrial plants (Eglinton and Hamilton, 1967). The majority of the samples (67 %) have dominant *n*-alkane chain lengths of C_{29} and C_{31}. For the remaining 33 % of the samples, concentrated between 6 and 1.1 cal kyr BP, the dominant chain length switched to *n*-C_{25}, indicating a higher *n*-alkane input from submerged macrophytes (Ficken et al., 2000). The *n*-C_{25} are unlikely to be sourced from mosses, as mosses are rare in subtropical peatland environments (Baker et al., 2016). Instead, the C_{25} is likely mainly derived from aquatic plants, which produce mid-chain *n*-alkanes as dominant homologues (C_{20}–C_{25}; Ficken et al., 2000). This increase of *n*-alkanes sourced from aquatic plants *c*. 6–1.1 cal kyr BP is unlikely to have had any impact on the isotopic composition of the long-chain *n*-alkanes (C_{29} and C_{31}) as these are minor components in aquatic plants (e.g. Aichner et al., 2010). Therefore, we interpret the $\delta^{13}C_{wax}$ as changes in the C_3/C_4 ratio of terrestrial higher plants.

Grasses exhibiting the C_4 or C_3 photosynthetic pathway in South Africa are largely geographically separated, with C_4 grasses dominant within the SRZ and C_3 grasses more prevalent in the YRZ, WRZ and at higher altitudes (Vogel et al., 1978). As C_4 grasses require less water to fix CO_2, thus having greater water-use efficiency than C_3 grasses, C_4 photosynthesis is favored in arid regions (e.g. Downes, 1969; Osborne and Sack, 2012). C_4 grasses also have the potential to achieve higher rates of photosynthesis than C_3 particularly at high irradiance and temperature levels (Black et al., 1969; Monteith, 1978), as their more efficient carbon fixation has a higher energy demand (Sage, 2004). Today growing season temperatures are a controlling factor for the distribution of C_4 and C_3 grasses (with C_4 grasses having an advantage over C_3 grasses at higher temperatures; Sage et al., 1999). Consequently C_4 grasses are mainly found in warm and dry environments such as the African savannas (Beerling and Osborne, 2006). Furthermore, under reduced atmospheric (i.e. glacial) CO_2, the higher carbon fixation efficiency of C_4 grasses provides an important advantage over C_3 grasses (Sage, 2004; Pinto et al., 2014). Previous palynological studies indicate that the dominant components of the pollen assemblage at Mfabeni are Poaceae and Cyperaceae (Finch and Hill, 2008). Although Cyperaceae species can be either C_3 or C_4, most Cyperaceae in eastern South Africa (67 %) are of the C_4-type (Stock et al., 2004). The C_4 vegetation at Mfabeni is thus mostly Poaceae or Cyperaceae from the sedge and reed fen. The C_3 vegetation at Mfabeni is comprised of arboreal taxa from the swamp forest (e.g. Myrtaceae and *Ficus*) and locally distributed *Podocarpus* (Finch and Hill, 2008; Venter, 2003). Shifts to higher $\delta^{13}C_{wax}$ values (more C_4-type vegetation) at Mfabeni could indicate an expansion of grassland (at the expense of arboreal taxa), or a shift from C_3 to C_4 grasses, resulting from: i) less precipitation, iii) a longer/more intense dry season, iv) heightened ET, v) reduced water table height, vi) higher temperatures, vii) reduced atmospheric CO_2, or viii) increased insolation levels (or any combination of the above).

The δD_{wax} reflects the δD_{precip}, ET and vegetation type. The δD_{precip} can be influenced by changes in air temperature, with an estimated temperature effect of *c*. 0.5‰ per 1°C for $\delta^{18}O_{precip}$ (Dansgaard, 1964). The maximum estimated temperature change of *c*. 6 °C in the SRZ of South Africa from the LGM to Holocene (Gasse et al., 2008), would thus correspond to a change in $\delta^{18}O_{precip}$ of 3‰. Conversion to changes in δD_{precip} using the global meteoric water line would thus lead to a potential LGM to Holocene δD_{precip} enrichment of 24‰ (Craig, 1961). However, the Mfabeni δD_{wax} record shows a depletion in δD_{wax} from the LGM to the Holocene, rather than an enrichment. The observed glacial δD depletion is therefore a conservative estimate. Consequently, changes in temperature from the LGM to the Holocene did not exert a dominant control on Mfabeni δD_{wax}.

Changes in vegetation type (C_3/C_4) have the potential to reduce or exaggerate shifts in δD_{wax}. There are differences in the apparent fractionation (the integrated isotopic fractionation between precipitation and plant-wax lipids) between plant types using different photosynthetic pathways. C_3-type shrubs and trees fractionate the least, C_4-type grasses slightly more, while C_3-type grasses show the highest apparent fractionation (Sachse et al., 2012). The difference in δD_{wax} between dicots (C_3, shrubs, trees and forbs) and monocots (C_4, grasses) is likely the result of leaf architecture and the nature of water movement in the leaf. Monocots display progressive evaporative enrichment along parallel veins along the leaf, which does not occur in dicots. This grass-blade enrichment results in higher δD_{wax} values in C_4 grasses (Helliker and Ehleringer, 2000). However, recent data suggest that the effect of C_3-tree to C_4-grass vegetation type changes on δD_{wax} is likely relatively small (Collins et al., 2013; Vogts et al., 2016).

The δD_{precip} is strongly controlled by the 'amount effect', where there is a negative correlation between monthly precipitation amount and δD_{precip} (Dansgaard, 1964). Close to the equator, passage of the tropical rainbelt can result in precipitation that is extremely depleted in D. Conversely, in arid regions, rainfall tends to be enriched in D because of enhanced evaporation of the raindrops as they fall (Risi et al., 2008). Studies investigating the present-day relationship between precipitation amount and the isotopic variations in rainfall indicate shifts in $\delta^{18}O$ of up to 15‰ (*c*. 120‰ in δD) with the passage of the tropical rainbelt and shifts in $\delta^{18}O$ of 7‰ (*c*. 56‰ in δD) with the passage of convective storms (Gat et al., 2001). During times of heightened ET and/or lower precipitation amount, soil waters become enriched in D (Sprenger et al., 2017). In addition, under conditions of low ambient relative humidity, leaf water becomes enriched in D through increased transpiration (Kahmen et al., 2013). Large values of isotopic enrichment (*c*. 40‰ in $\delta^{18}O$, 180‰ in δD) are associated with the effects of evaporation (e.g. Cappa et al., 2003).

Mfabeni has high rates of ET, which can equal, or even exceed precipitation during dry periods (Grundling et al., 2015). Consequently, both precipitation amount and ET are likely to control the isotopic composition of soil and leaf waters, and subsequently of the leaf waxes at Mfabeni. High δD_{wax} values at Mfabeni likely result from decreased summer precipitation amount and/or heightened ET. The similarity between the δD_{wax} pattern and the regional precipitation/aridity stacks (Fig. 4d & e; Chevalier and Chase, 2015; 2016) supports the inference that precipitation amount and ET drive Mfabeni δD_{wax}. Furthermore, this similarity indicates that the hydrological fluctuations in the Mfabeni record represent hydrological change at a broader spatial scale (Fig. 4c–e), but also suggest that the pollen-based precipitation stacks may also include an element of ET variability.

6.2 Climatic and environmental conditions at Mfabeni over the last 32 cal ka BP

The $\delta^{13}C_{wax}$, δD_{wax} and P_{aq} data from Mfabeni indicate that the vegetation, hydrology and the water table varied considerably over the last 32 cal ka BP (Fig. 4 &. 5). The high $\delta^{13}C_{wax}$ values during the LGM indicate that the vegetation was likely dominated by more drought-tolerant C_4 plant types (Fig. 4b). Similar LGM $\delta^{13}C_{wax}$ depletion was observed previously at Mfabeni (Fig. 4h; Baker et al., 2017). Drier conditions during the LGM correspond with low P_{aq} values that indicate a higher relative contribution of terrestrial-over-aquatic *n*-alkanes, likely a consequence of a lower water table (Fig. 4f). The high δD_{wax} values during the LGM suggest decreased precipitation amount and/or higher ET, which are both consistent with a drier environment (Fig. 4c). We cannot completely rule out the possible impact of increased drainage of the peatbog during the LGM due to low eustatic sea level (Grundling et al., 2013). A lower water table during the LGM would likely serve to further soil water D enrichment. Nevertheless, the fact that the peat continued to grow during the LGM suggests that the sea level effect was minor. The organic geochemical proxies agree with palynological data indicating regional grassland dominance (high Poaceae, Cyperaceae and Asteraceae) with low amounts of arboreal taxa (Fig. 6; Finch and Hill, 2008). Regional aridity and increased wind strength during the LGM at Mfabeni are also indicated by increased mean grain size of the lithogenic sediment fraction (Fig. 4g), and the modal grain size of the distal aeolian component (Humphries et al., 2017). Evidence for reduced precipitation (from the regional precipitation stack; Fig. 4d) and high aridity (from the regional aridity stack; Fig. 4e) during the LGM, provide evidence that the dry conditions at Mfabeni appear to be part of a wider eastern South African pattern (Fig. 4d & e).

The shift to more negative $\delta^{13}C_{wax}$ values following the LGM, at *c*. 19 cal ka BP, indicating that the vegetation at Mfabeni changed to more C_3-type (Fig. 4b), is also evident in Mfabeni core SL6 (Fig. 4h; Baker et al., 2017). This change is thus likely representative of a C_4–C_3 change across the peat bog. The palynological record indicates no shift towards arboreal taxa at this time but instead a continuation of grasslands (Fig. 6a & b; Finch and Hill, 2008). A decrease in Cyperaceae percentages (as most Cyperaceae is of C_4 type), may be responsible for the C_4 to C_3 shift observed in the $\delta^{13}C_{wax}$ record, but the gradual nature of the Cyperaceae decrease points to an additional driver (Fig. 6c). The shift is more likely the result of a switch from C_4 to C_3 grasses. If temperature was driving the vegetation shifts at Mfabeni, we would expect a shift from C_3 to C_4 grasses from the LGM to the Holocene (with a *c*. 6°C increase in temperature). Nevertheless, the LGM to Holocene shift from C_4 to C_3 grasses suggests that temperature did not drive the vegetation change at Mfabeni. We suggest that the shift from C_4 to C_3 grasses may have been caused instead by i) more precipitation, ii) a shorter/less intense dry season, iii) lower ET, and/or iv) increased water table height. Furthermore, with C_3 vegetation favored under lower insolation conditions, a decrease in local summer insolation from the LGM to Holocene (Fig. 4a) could have played a role in driving the vegetation shifts.

After *c*. 19 cal ka BP, the $\delta^{13}C_{wax}$ values continue to decrease to -29‰ until they stabilize at *c*. 14 cal ka BP. This trend in $\delta^{13}C_{wax}$ values between *c*. 19 and 14 cal kyr BP, indicating an expansion of C_3 vegetation, corresponds well with the $\delta^{13}C_{wax}$ record from Mfabeni core SL6 (Baker et al., 2017; Fig. 4b & 4h). There are, however, some minor differences between the two $\delta^{13}C_{wax}$ records. We attribute these to small-scale variations in vegetation across the peatbog, the lower sampling resolution of core SL6 and to dating uncertainties in both records. The shift to lower $\delta^{13}C_{wax}$ values at *c*. 19 cal ka BP occurs at the same time as a rise in the water table as documented by an increase in P_{aq} values (Fig. 4f). An abrupt increase in precipitation amount and a decrease in aridity is evident in the precipitation and aridity stacks at *c*. 19 cal ka BP. All proxy records for precipitation (the regional stacks and the Mfabeni δD_{wax} data; Fig. 4) strongly suggest a switch to wetter conditions after *c*. 19 cal ka BP.

The $\delta^{13}C_{wax}$ values between 14–5 cal kyr BP reflect a stable period of C_3-type vegetation (Fig. 4b). At the same time, gradually decreasing δD_{wax} values indicate increasing humidity. The gradual increase in precipitation is also evident in the precipitation stack, but this trend is interrupted by an abrupt return to aridity at *c*. 14.2 cal ka BP, coinciding with the Antarctic Cold Reversal (Chase et al., 2017). This abrupt arid event is only evident in one sample at Mfabeni and thus higher resolution sampling is needed across this interval. The aridity stack indicates low aridity during this interval, but high variability suggests a complex interplay between high ET (from increased temperatures, resulting in less effective precipitation) and generally more precipitation (Fig. 4e). Pollen data from Mfabeni provide evidence for an expansion of arboreal type vegetation at *c*. 12 cal ka BP (Fig. 6a; Finch and Hill, 2008). The pollen data thus suggest the establishment of swamp forest vegetation during the early Holocene, indicative of a moist climate (Fig. 6a). Mfabeni aeolian sediment flux is low and stable throughout this period, also suggesting a moist climate (Humphries et al., 2017). The moist climate likely resulted in vegetated dunes, reducing the amount of material available for aeolian transport. The relatively high P_{aq} values between 14–5 cal kyr BP indicate a high and stable water table at this time (Fig. 4f). Elevated total organic carbon percentages within Mfabeni core SL6 during the Holocene, also suggest increased water levels (Baker et al., 2017).

Between *c*. 5–0 cal kyr BP several high-amplitude millennial-scale C_3/C_4 vegetation changes are evident superimposed on an overall shift from predominantly C_3 to more C_4-type vegetation towards the present-day (Fig. 5b). This variability contrasts with the more gradual C_4/C_3 vegetation transition from the glacial period to Holocene. The $\delta^{13}C_{wax}$ values from Mfabeni core SL6 between *c*. 6–1 cal kyr BP also indicate a period of predominantly C_4-type vegetation, implying arid conditions during this time (Baker et al., 2017; Fig. 4h). A similar pattern of a long-term trend with superimposed short-term variability is visible in the in δD_{wax} record. The general enrichment in D reflects gradual drying, punctuated by millennial-scale pulses of aridity, with the most pronounced arid event at *c*. 2.8 cal ka BP (Fig. 5c). Counterintuitively, the high abundance of *n*-C_{25} alkanes and high but variable P_{aq} values between *c*. 5–0 cal kyr BP indicate a generally high water table, interrupted by brief periods of a lower water table (Fig. 5d). After 2.3 cal ka BP, both $\delta^{13}C_{wax}$ and δD_{wax} values become higher and P_{aq} values lower (Fig. 5b–d). This suggests increased C_4-type vegetation cover, decreased summer precipitation amount and/or higher ET and low water table levels. A slight increase in precipitation followed by gradually decreasing precipitation over the last *c*. 5 ka is evidenced in the precipitation stack (Fig. 4d). This initial increase in precipitation at *c*. 5 cal ka BP corresponds to an abrupt decrease in aridity (Fig.

4d & e). The increased variability observed in our records between 5–0 cal kyr BP could be an artefact of the high temporal resolution of our record during this interval (~220 vs ~700 years per sample for the remainder of the record). Nevertheless, (Fig. 4d) other data from the region (e.g. Baker et al., 2017, Humphries et al., 2017; 2016, Finch and Hill, 2008, Neumann et al., 2010) also indicate climatic instability and arid climatic conditions during the last *c*. 5 cal ka BP, suggesting that the observed variability is likely real (Fig. 5e).

It is interesting that modern δD_{wax} values and those during the LGM appear similar (Fig. 4c), implying similarly arid conditions during both periods. The southern aridity stack also indicates extremely arid conditions during the last few thousand years and the authors stress the importance of temperature in controlling aridity (Fig. 4e; Chevalier and Chase, 2016). It is possible that modern high mean annual temperatures drove these modern-day δD_{wax} values to appear similar to those from the LGM. High modern day temperatures, increase ET and result in less 'effective precipitation' and arid conditions, even when rainfall is high (Cheavlier and Chase, 2016). During the LGM, lower temperatures would have reduced ET, leading to apparent humid conditions, despite reduced rainfall amount.

6.3 Climate driving mechanisms

Modern observations suggest that high SSTs within the Mozambique Channel and Agulhas Current induce increased evaporation (e.g. Walker, 1990), resulting in higher rainfall in the SRZ (Tyson, 1999). Variations in local SSTs are thus thought to be an important driver of hydroclimate in eastern South Africa. This mechanism may also play a role on longer timescales. Indeed, Chevalier and Chase (2015) invoke SSTs as the dominant driver of precipitation variability during the LGM. Mfabeni vegetation and hydrology reconstructions over the last 32 cal ka BP do not show a clear relationship with changes in southwest Indian Ocean SSTs (Fig. 4j, Sonzogni et al., 1998). For example if SSTs drove the climate at Mfabeni then the abrupt shift to more C_3 type vegetation and the gradual shift to a wetter climate at *c*. 19 cal ka BP would be expected to correspond with an increase in SSTs. This is not the case, and SSTs do not increase until *c*. 15.7 ka (Sonzogni et al., 1998; Fig. 4). The lowest temperatures within the Mozambique Channel correspond to Heinrich Event 1 (SSTs *c*. 3°C colder than present day), an event which is not evident as a particularly arid period in the Mfabeni dataset. Mozambique Channel SSTs thus do not fully explain the variability observed in the records comprising the precipitation stack. These differences, as proposed previously by Chevalier and Chase (2015), suggest that SST variability is unlikely to be the sole driver of the changes in hydroclimate within this part of the SRZ. Chevalier and Chase (2015) proposed that the differences observed between SSTs and the records comprising the precipitation stack is due to the modulation of precipitation by the position of the westerlies.

We attribute the arid climate and the associated expansion of drought tolerant C_4 plants and a low water table at Mfabeni during the LGM, in part, to a northward displacement of the westerlies, the SIOCZ and the subtropical high-pressure cell, shifting the hydroclimate to a more evaporative regime, where ET exceeds precipitation. In addition, lower SSTs (Fig. 4j) in the Mozambique Channel at this time likely reduced moisture availability. It is possible that the combination of a northward displacement of these three systems (the westerlies, SIOCZ and subtropical high-pressure cell) and lower SSTs shifted the fine balance between precipitation and ET at Mfabeni towards higher ET rates during the LGM.

Palaeoenvironmental studies (e.g. Lamy et al., 2001; Lamy et al., 2010; Stuut and Lamy, 2004), climate model simulations (e.g. Rojas et al., 2009; Toggweiler et al., 2006) and theoretical models (e.g. Cockcroft et al., 1987) provide evidence for an equatorward migration and strengthening of the southern hemisphere westerlies in response to the increased extent of Antarctic sea ice during the LGM. Records from the present WRZ such as Elands Bay Cave (Baxter, 1996), Pakhuis Pass (Scott, 1994) and Driehoek Vlei (Meadows and Sugden, 1993) indicate increased winter rainfall, interpreted as a northward shift and strengthening of the westerlies during the LGM (Chase and Meadows, 2007). An equatorward migration of the westerlies may have expanded the limit of the WRZ in South Africa northward, to around 25°S in the west and 30°S in the east (Cockcroft et al., 1987). This would have put Mfabeni (at 28°S) within the range of the southern westerlies. Although during the LGM the westerlies were in a more northerly position, and had the potential to provide rainfall (via the passage of more cold fronts; Nkoana et al., 2015), we do not see any evidence for increased precipitation at Mfabeni. Today mid-latitude cyclones (frontal systems; Fig. 1b) associated with the westerlies trigger rainout of atmospheric moisture, sourced from the Indian Ocean and Agulhas Current, during the winter months (Gimeno et al., 2010). However, the co-occurring subtropical high-pressure cell over the South African interior may have limited the amount of moisture advection towards Mfabeni, thus even with increased cyclone occurrence, arid conditions persisted. Furthermore, with a northerly displaced subtropical high-pressure cell inhibiting monsoonal penetration, the duration of the dry season at Mfabeni may have been extended, shortening the rain season and heightened ET rates.

A northward migration and strengthening of the westerlies is also associated with a northerly displaced and weaker South Indian Anticyclone (Fig. 1; Cohen and Tyson, 1995). A weakening of the western portion of the South Indian Anticyclone results in a northeastward shift of the SIOCZ (and the rain-bearing cloud band associated with TTTs; Cook, 2000). This northeastward shift results in higher precipitation over coastal Africa (around 15°N) and Madagascar and lower than normal precipitation to the south, in eastern South Africa (Cook, 2000). We propose that a northeastward shift of the SIOCZ during the LGM may have also played a key role in driving aridity at Mfabeni.

The latitudinal position of the subtropical high-pressure cell is highly correlated to rainfall variability along the eastern coast of South Africa (Dyson and van Heerden, 2002). Multivariate analysis of zonal moisture fluxes in South Africa indicates that the latitudinal position of the subtropical high-pressure cell directly controls the amount of moisture advection (monsoonal penetration) towards the southern African interior during the summer months (Vigaud et al., 2009). When the cell is shifted southward, during the summer, the tropical easterlies are able to penetrate further inland, resulting in higher continental moisture availability (Vigaud et al., 2009). Conversely, when the cell is shifted northward, during the winter, monsoonal circulation south of 25°S is impeded, creating a deficit in moisture advection from the ocean to the continent (Tyson and Preston-Whyte, 2000; Vigaud et al., 2009). A more northerly location of the subtropical high-pressure cell, during the LGM, would have lengthened the dry season, resulting in aridity at Mfabeni.

We suggest that the shift to more humid conditions at *c*. 19 cal ka BP was related to the retreat of the westerlies, the subtropical high-pressure cell and the SIOCZ, as Antarctic sea ice began to retreat poleward (Fig. 4k), allowing an increased influence of the moist tropical easterlies. With the subtropical high-pressure cell further south, stronger easterly flux from the Indian Ocean likely enhanced the development of TTTs in the region leading to increased precipitation. This shift at *c*. 19 cal ka BP was unlikely driven by a change in local summer insolation because insolation was decreasing at this time. We suggest that the abrupt shift to more C_3 vegetation was a non-linear response to increasing moisture availability in the region (Fig. 4c). Precipitation amount may have reached a critical threshold at *c*. 19 cal ka BP for the establishment of C_3 type vegetation, resulting in the observed abrupt vegetation shift (Fig. 4b).

Between 14–5 kyr BP, a reduced extent of Antarctic sea ice (Fig. 4k & 5g), resulted in a more poleward position of the westerlies and the subtropical high-pressure cell. The diminished effect of the westerlies and the subtropical high-pressure cell in eastern South Africa at this time permitted the tropical systems (easterlies), to dominate the climatic regime at Mfabeni. With a strengthened (but poleward displaced) South Indian Anticyclone the SIOCZ was likely situated over Mfabeni resulting in increased rainfall. Strong easterly flux would have increased the development of TTTs in the region, resulting in higher humidity at Mfabeni. Increasing humidity at Mfabeni during the Holocene, corresponds with increasing southern hemisphere summer insolation (Fig. 4a). The importance of insolation for South African climate variability during the late Quaternary has been suggested before (e.g. Partridge et al., 1997; Simon et al., 2015). Our results support the hypothesis that insolation control on precipitation variability was only significant during the Holocene (e.g. Schefuß et al., 2011; Chevalier and Chase, 2015). We suggest that direct local insolation forcing is only dominant in this region when the westerlies and subtropical high-pressure cell are located far south, which allows monsoonal precipitation to penetrate into the continent during the summer months.

To explain the millennial-scale climatic variability over the glacial-interglacial transition within their central and eastern African sites (which also includes Mfabeni), Chevalier and Chase (2015) and Chase et al. (2017) suggest that this region may be influenced by the position and the intensity of the westerlies, and the interactions between the westerlies and the tropical easterlies (resulting in TTT development). We highlight the importance of the location of TTT development (i.e the SIOCZ) and stress the interconnections between TTT development, the latitudinal position of the westerlies and the subtropical high-pressure cell on glacial-interglacial timescales.

After *c.* 5 cal ka BP, palaeoenvironmental records from both the WRZ and YRZ, such as from Verlorenvlei (Fig. 1; Fig. 5f; Carr et al., 2015), Seweweekspoort (Fig. 1; Fig. 4i; Chase et al., 2017), Klaarfontein (Fig. 1; Meadows and Baxter, 2001), Cecilia Cave (Fig. 1; Baxter, 1989) and Eilandvlei (Wündsch et al., 2018), document increased moisture availability, implying a recurring more northerly location of the westerlies. Chevalier and Chase et al. (2015) propose that increased precipitation in the WRZ during the late Holocene was due to both the warmer interglacial climate and the northward expansion of the westerly storm tracks. Although no indication for an increase in sea ice is evident from EPICA salt concentration data (Fig. 4k), diatom data (*Fragilariopsis curta* and *F. cylindrus*) from PS2090/ODP1094 in the southern South Atlantic document an increase in sea ice during the late Holocene (Fig. 5g), which may have pushed the southern westerlies equatorward. In addition, climate modelling results imply a northward shift of the southern westerlies at this time (Hudson and Hewitson, 2001). Consequently, in a comparable way to the LGM, the increased sea ice during the late Holocene (Fig. 5g), may have displaced (and strengthened) the westerlies, the South African high-pressure system and the SIOCZ equatorward, resulting in higher aridity at Mfabeni. A slight decrease in Mozambique Channel SSTs may have also played a role in the generally arid climate at Mfabeni during the last *c*. 5 cal ka BP (Fig. 4j; Sonzogni et al., 1998). Interestingly, the hydrological variability at Mfabeni (Fig. 5c) during the last *c*. 5 cal ka BP, is not present in the central and eastern South African precipitation stack (Fig. 4d). We attribute this to the highly sensitive balance between ET and precipitation at Mfabeni (Grundling et al., 2015), and the fact that the precipitation stack smooths local hydrological variability.

It is possible that anthropogenic influences also played a role in shaping the environment at Mfabeni, at least, during the late Holocene. However, unequivocal agricultural and exotic pollen indicators are absent from the pollen record and although pollen data indicate that forest decline occurred during the late Holocene, it is unclear whether this was related to human influence or regional climate change (Fig. 6; Finch and Hill, 2008). The forest decline could have affected the water table and increased the relative amount of C_4-type vegetation. The appearance of *Morella* and *Acacia* in the late Holocene may indicate the development of open vegetation or secondary forest due to fire disturbance (Fig. 6e; Finch and Hill, 2008). Human activities or climate change may be responsible for changes in fire regime. With no palaeo-charcoal data available for Mfabeni yet, no direct evidence for increased fire activity during the late Holocene exists. In addition, the palaeoenvironmental evidence available suggests that the arid conditions during the late Holocene were regional in nature (Scott, 1999; 2003; Humphries et al., 2016, Neumann et al., 2010). Thus, any human activity was unlikely the primary cause of the late Holocene regional aridity and the large magnitude of environmental changes observed at Mfabeni.

Today ENSO activity is one of the most important driving mechanisms for inter-annual climatic variability in South Africa. Southern Africa's seasonal rainfall is linked to ENSO, with dry (wet) conditions associated with El Niño (La Niña) events (Archer et al., 2017; Mason and Jury, 1997). Interannual variability in the strength and position of the SIOCZ is linked to ENSO variability (Cook, 2000). During La Niña years, the SIOCZ is located over the continent, resulting in wet conditions in eastern South Africa. During El Niño, the SIOCZ shifts northeastward over the Indian Ocean and as a consequence, dry conditions prevail in eastern South Africa (Lindesay, 1988; Cook, 2001; Hart et al., 2018). Furthermore, during El Niño events, a northward shift of the westerlies may occur, which could increase rainfall over western South Africa but lead to aridity in the east (i.e. at Mfabeni; Lindesay, 1988). Palaeoenvironmental studies in the Pacific Basin and South America indicate that during the early Holocene El Niño events were smaller and occurred less frequently, with a shift to stronger ENSO activity after *c*. 5 cal ka BP (Fig. 5h, Moy et al., 2002; Huffman, 2010; Rodbell et al., 1999; Sandweiss et al., 1996). It is difficult to disentangle the possible potential drivers of climate variability during the last *c*. 5 cal ka BP at Mfabeni. We therefore invoke a possible combination of northerly-displaced westerlies, lower SSTs and the impact of ENSO variability as potential climatic drivers during this time.

7. Conclusions

Compound specific carbon and hydrogen isotope data and *n*-alkane distributions (P_{aq}) from Mfabeni peatbog are used to reconstruct climatic conditions, over the last 32 cal ka BP in eastern South Africa. The LGM at Mfabeni was characterized by a high contribution of C_4 grasses, low precipitation amount/high ET and a low water table. During the LGM, increased Antarctic sea ice extent led to an equatorward displacement (and strengthening) of the southern hemisphere westerlies, the SIOCZ and the subtropical high-pressure cell, which may have extended the length and increased the intensity of the dry season, as well as shifted the location of TTT formation northeast of Mfabeni. Between *c*. 19–5 cal kyr BP an expansion of C_3-type vegetation occurred, with more rainfall and a higher water table at Mfabeni. At *c*. 19 cal ka BP, Antarctic sea ice decreased, which resulted in a southward retreat of the westerlies, the SIOCZ and the subtropical high-pressure cell. This retreat combined with an increase in local summer insolation, after *c*. 12 cal ka BP, resulted in more precipitation and an increased wet season length at Mfabeni. When the westerlies, the SIOCZ and the subtropical high-pressure cell were in their southernmost position (*c*. 14–5 cal kyr BP), local insolation became the dominant control on Mfabeni climate, leading to stronger convection and enhanced monsoonal precipitation from the tropical easterlies. The late Holocene (*c*. <5 cal ka BP) was characterized by increased environmental instability and increasingly arid conditions. We attribute these trends to concurring low SSTs, and the recurring influence of the southern westerlies and/or heighted ENSO activity.

The Mfabeni record indicates that climate and environmental variability in eastern South Africa over the last 32 cal ka BP were driven by a combination of i) enhanced/reduced moisture transport by the tropical easterlies, driven by variations in southern hemisphere summer insolation, and ii) latitudinal displacements (and the strengthening/weakening) of the westerlies, the SIOCZ and the subtropical high-pressure cell. With the expansion and retreat of Antarctic sea ice ultimately responsible for the displacement of these systems, we invoke high-latitude climate forcing as an important driver of climate in eastern South Africa.

Data availability: Supplementary data for the depth-age model **(S1)** is available with this manuscript. A new depth-age model of core MF1 (Finch and Hill, 2008), produced by Bacon, can be found within the supplementary information **(S2)**. Other data is available on PANGAEA.

Author contributions: CM and ES conducted $\delta^{13}C_{wax}$ and δD_{wax} analyses. Interpretation was carried out by CM, JF, TH, FP, MH, MZ and ES.

Competing interests: The authors declare no competing financial interests.

Acknowledgements: This research was funded by the Bundesministerium für Bildung und Forschung (BMBF; RAiN project 03G0840A/B) and NRF Grant 84431 (JF). We thank R. Kreutz for assistance with $\delta^{13}C_{wax}$ and δD_{wax} data acquisition and L. Jonkers for helpful input with manuscript writing.

Figure captions

Figure 1. Map of South Africa in austral summer **(a)** and winter **(b)** showing the major oceanic and atmospheric currents and the position of the Congo Air Boundary (CAB). H (L) = high (low)-pressure systems. BC = Benguela Current. AC = Agulhas Current. Rainfall zones are shown in **(a)**: WRZ = winter rainfall zone, YRZ = year-round rainfall zone, SRZ = summer rainfall zone. SIA = South Indian Anticyclone. SAA = South Atlantic Anticyclone. SIOCZ = South Indian Ocean Convergence Zone. Note, the westerlies move north during austral winter and the high-pressure system dominates over much of the continent, suppressing rainfall in the SRZ. Squares represent the key study sites mentioned in the text (and shown in Fig. 4 and 5): **a)** MD79257 (Sonzogni et al., 1998). **b)** Mfabeni, this study (red

square). **c)** Lake St Lucia (Humphries et al., 2016). **d)** Seweweekspoort (Chase et al., 2017). **e)** Cecilia Cave (Baxter, 1989). **f)** Klaarfontein (Meadows and Baxter, 2001) and Verlorenvlei (Carr et al., 2015), one location. Figure modified from Gasse et al. 2008.

Figure 2. Mfabeni peatland and its regional geomorphological features, indicating the location of core MF4-12 (red circle, this study) and the location of core SL6 (black circle, Baker et al., 2014; 2016; 2017). Map is courtesy of B. Gijsbertsen, UKZN Cartography Unit.

Figure 3. Depth-age model of core MF4-12 produced using Bacon, based on 24 ^{14}C AMS dates (S1). Blue symbols are AMS dates and grey shading indicates 95% confidence interval on the mean age (red line).

Figure 4. Climate and environmental change at Mfabeni compared with regional records and orbital insolation. **a**) December-January-February (DJF) insolation for 28°S (blue line; Laskar et al., 2011). **b**) Stable carbon isotope composition (weighted mean) of C_{29}–C_{31} *n*-alkanes from Mfabeni, reflecting changes in C_3/C_4 vegetation type. **c**) Hydrogen isotope composition (weighted mean) of C_{29}–C_{31} *n*-alkanes from Mfabeni, reflecting changes in precipitation amount and ET. Red is the δD_{wax} corrected for ice volume changes. Error bars on isotope data reflect analytical uncertainty of duplicate analyses. **d**) Central and eastern South African regional precipitation stack (red line; Chevalier and Chase, 2015). **e**) Southern African regional aridity stack (Chevalier and Chase, 2016). **f**) P_{aq} at Mfabeni, indicating the amount of aquatic vs. terrestrial *n*-alkanes (high/low water table). **g**) Mean grain size data of the lithogenic sediment fraction from Mfabeni (Humphries et al., 2017). **h)** Mfabeni core SL6 stable carbon isotope composition (weighted mean) of C_{29}–C_{31} *n*-alkanes (Baker et al., 2017). **i)** Combined nitrogen isotope data from Seweweekspoort rock hyrax middens, reflecting changes in humidity (Chase et al., 2017). **j**) $U^{K'}_{37}$ derived SSTs from core MD79257 in the Mozambique Channel (Sonzogni et al., 1998). **k**) Sea salt sodium concentrations from the EPICA DML ice core in Antarctica, reflecting changes in sea ice coverage (Fischer et al., 2007). The two Mfabeni samples with CPI values of *c*. 2 are highlighted in red (4b & c). Blue shading = Mfabeni wet, orange = Mfabeni arid.

Figure 5. Comparison of Mfabeni data with other records of environmental variability over the last 15 cal kyr BP. **a)** DJF insolation for 28°S (black line; Laskar et al., 2011). **b)** Carbon isotope composition (weighted mean) of C_{29}–C_{31} *n*-alkanes from Mfabeni, reflecting changes in C_3/C_4 vegetation type. **c)** Hydrogen isotope composition (weighted mean) of C_{29}–C_{31} *n*-alkanes from Mfabeni, reflecting changes in summer precipitation amount and ET. **d)** P_{aq} at Mfabeni, indicating the amount of aquatic vs. terrestrial n-alkanes (high/low water table). Blue dashed lines highlight trends. **e)** Mfabeni

calcium/scandium ratio, indicating changes in water table (Humphries et al., 2017). **f)** Bulk carbon isotope data from Verlorenvlei (Carr et al., 2015). **g)** An estimation of the extent of Antarctic sea ice based on the abundance of *Fragilariopsis curta* and *Fragilariopsis cylindrus* at site PS2090/ODP1094 (SW of Cape Town; Bianchi and Gersonde, 2004). **h)** Red colour intensity time-series from Laguna Pallcacocha. High values are light coloured inorganic clastic laminae, which were deposited during ENSO-driven episodes (Moy et al., 2002). The Mfabeni sample with a CPI value of *c*. 2 is highlighted in red (5b & c).

Figure 6. Summary figure highlighting the main climate phases and driving mechanisms at Mfabeni. All pollen data is from Finch and Hill (2008). Note, the new age model for pollen % data is in the supplementary material (S2). **a)** *Podocarpus* % data from Mfabeni. **b)** Poaceae % data from Mfabeni. **c)** Cyperaceae % data from Mfabeni. **d)** Asteraceae % data from Mfabeni. **e)** *Morella serrata* % data from Mfabeni. Poaceae and Cyperaceae were excluded from the regional pollen sum so their percentages are based on total pollen frequencies. *Podocarpus*, Asteraceae and *M. serrata* percentages are based on regional frequencies. See Finch and Hill (2008) for more details. **f)** Stable carbon isotopic composition (weighted mean) of C_{29}–C_{31} *n*-alkanes from Mfabeni. **g)** Hydrogen isotope composition (weighted mean) of C_{29}–C_{31} *n*-alkanes from Mfabeni. Red is the δD_{wax} corrected for ice volume changes. The two Mfabeni samples with CPI values of *c*. 2 are highlighted in red. Blue shading = Mfabeni wet, orange = Mfabeni arid.

References

Archer, E.R.M., Landman, W.A., Tadross, M.A., Malherbe, J., Weepener, H., Maluleke, P., Marumbwa, F.M.: Understanding the evolution of the 2014–2016 summer rainfall seasons in southern Africa: Key lessons, Climate Risk Management, 16, 22-28, 2017.

Aichner, B., Herzschuh, U., Wilkes, H.: Influence of aquatic macrophytes on the stable carbon isotopic signatures of sedimentary organic matter in lakes on the Tibetan Plateau, Org. Geochem., 41, 706-718, 2010.

Baker, A., Routh, J., Blaauw, M., Roychoudhury, A.N.: Geochemical records of palaeoenvironmental controls on peat forming processes in the Mfabeni peatland, Kwazulu Natal, South Africa since the Late Pleistocene, Palaeogeogr. Palaeoecol., 395, 95-106, 2014.

Baker, A., Routh, J., Roychoudhury, A.N.: Biomarker records of palaeoenvironmental variations in subtropical Southern Africa since the late Pleistocene: Evidences from a coastal peatland, Pleistocene. Palaeogeogr. Palaeoecol., 451, 1-12, 2016.

Baker, A., Pedentchouk, N., Routh, J., Roychoudhury, A.N.: 2017. Climatic variability in Mfabeni peatlands (South Africa) since the late Pleistocene, Quaternary Sci.Rev., 160, 57-66, 2017.

Barker, P.A., Leng, M.J., Gasse, F., Huang, Y.: Century-to-millennial scale climatic variability in Lake Malawi revealed by isotope records, Earth Planet. Sci.Lett., 261, 93-103, 2007.

Baxter, A.J.: Pollen analysis of a Table Mountain cave deposit. University of Cape Town, Cape Town. 1989.

Baxter, A.: Late Quaternary Palaeoenvironments of the Sandveld, Western Cape Province, South Africa, PhD, University of Cape Town, Cape Town, South Africa, 1996.

Beerling, D. J. and Osborne, C. P.: The origin of the savanna biome, Global Change Biology, 12, 2023-2031, 2006.

Bianchi, C., Gersonde, R.: Climate evolution at the last deglaciation: the role of the Southern Ocean, Earth Planet. Sci.Lett., 228, 407-424, 2004.

Blaauw, M., Christen, J.A.: Flexible paleoclimate age-depth models using an autoregressive gamma process, Bayesian Anal., 6, 457-474, 2011.

Black, C. C., Chen, T. M., and Brown, R. H.: Biochemical Basis for Plant Competition, Weed Science, 17, 338-344, 1969.

Braconnot, P., Otto-Bliesner, B., Harrison, S., Joussaume, S., Peterchmitt, J.Y., Abe-Ouchi, A., Crucifix, M., Driesschaert, E., Fichefet, T., Hewitt, C.D., Kageyama, M., Kitoh, A., Laîné, A., Loutre, M.F., Marti, O., Merkel, U., Ramstein, G., Valdes, P., Weber, S.L., Yu, Y., Zhao, Y.: Results of PMIP2 coupled simulations of the Mid-Holocene and Last Glacial Maximum – Part 1: experiments and large-scale features, Clim. Past, 3, 261-277, 2007.

Bray, E.E., Evans, E.D.: Distribution of n-paraffins as a clue to recognition of source beds, Geochim. et Cosmochim. Ac., 22, 2-15, 1961.

Cappa, C. D., Hendricks, M. B., DePaolo, D. J., and Cohen, R. C.: Isotopic fractionation of water during evaporation, Journal of Geophysical Research: Atmospheres, 108, 2003.

Carr, A.S., Boom, A., Chase, B.M.: Meadows, M.E., Grimes, H.L.: Holocene sea level and environmental change on the west coast of South Africa: evidence from plant biomarkers, stable isotopes and pollen, J. Paleolimnol., 53, 415-432, 2015.

Chase, B.M., Chevalier, M., Boom, A., Carr, A.S.: The dynamic relationship between temperate and tropical circulation systems across South Africa since the last glacial maximum, Quaternary Sci.Rev., 174, 54-62, 2017.

Chase, B.M., Meadows, M.E.: Late Quaternary dynamics of southern Africa's winter rainfall zone, Earth-Sci. Rev., 84, 103-138, 2007.

Chevalier, M., Chase, B.M.: Southeast African records reveal a coherent shift from high- to low-latitude forcing mechanisms along the east African margin across last glacial–interglacial transition, Quaternary Sci.Rev., 125, 117-130, 2015.

Chevalier, M., Chase, B.M.: Determining the drivers of long-term aridity variability: a southern African case study. J. Quaternary Sci., 31, 143-151, 2016.

Chevalier, M., Brewer, S., and Chase, B. M.: Qualitative assessment of PMIP3 rainfall simulations across the eastern African monsoon domains during the mid-Holocene and the Last Glacial Maximum, Quaternary Science Reviews, 156, 107-120, 2017.

Clark, P.U., Dyke, A.S., Shakun, J.D., Carlson, A.E., Clark, J., Wohlfarth, B., Mitrovica, J.X., Hostetler, S.W., McCabe, A.M.: The Last Glacial Maximum, Sci. J., 325, 710-714, 2009.

Cockcroft, M.J., Wilkinson, M.J., Tyson, P.D.: The application of a present-day climatic model to the late quaternary in southern Africa. Clim. Change, 10, 161-181, 1987.

Cohen, A. L. and Tyson, P. D.: Sea-surface temperature fluctuations during the Holocene off the south coast of Africa: implications for terrestrial climate and rainfall, The Holocene, 5, 304-312, 1995.

Collins, J.A., Schefuß, E., Mulitza, S., Prange, M., Werner, M., Tharammal, T., Paul, A., Wefer, G.: Estimating the hydrogen isotopic composition of past precipitation using leaf-waxes from western Africa, Quaternary Sci.Rev., 65, 88-101, 2013.

Collister, J.W., Rieley, G., Stern, B., Eglinton, G., Fry, B.: Compound-specific $\delta^{13}C$ analyses of leaf lipids from plants with differing carbon dioxide metabolisms. Org. Geochem., 21, 619-627, 1994.

Cook, K. H.: A Southern Hemisphere Wave Response to ENSO with Implications for Southern Africa Precipitation, Journal of the Atmospheric Sciences, 58, 2146-2162, 2001.

Cook, K. H.: The South Indian Convergence Zone and Interannual Rainfall Variability over Southern Africa, Journal of Climate, 13, 3789-3804, 2000.

Craig, H., Isotopic Variations in Meteoric Waters, Sci. J., 133, 1702-1703. 1961.

Dansgaard, W.: Stable isotopes in precipitation, Tellus, 16, 436-468, 1964.

Dedekind, Z., Engelbrecht, F. A., and van der Merwe, J.: Model simulations of rainfall over southern Africa and its eastern escarpment, Water SA, 42, 129-143, 2016.

Diefendorf, A.F., Freimuth, E.J.: Extracting the most from terrestrial plant-derived n-alkyl lipids and their carbon isotopes from the sedimentary record: A review, Org. Geochem., 103, 1-21. 2017.

DiNezio, P. N., Tierney, J. E., Otto-Bliesner, B. L., Timmermann, A., Bhattacharya, T., Rosenbloom, N., and Brady, E.: Glacial changes in tropical climate amplified by the Indian Ocean, Science advances, 4, 2018.

Downes, R. W.: Differences in transpiration rates between tropical and temperate grasses under controlled conditions, Planta, 88, 261-273, 1969.

Dupont, L., Caley, T., Kim, J.-H., Castañeda, I.S., Malaizé, B., Giraudeau, J.: Glacial-interglacial vegetation dynamics in South Eastern Africa coupled to sea surface temperature variations in the Western Indian Ocean, Clim. Past 7, 1209-1224, 2011.

Dupont, L.: Orbital scale vegetation change in Africa, Quaternary Sci.Rev., 30, 3589-3602, 2011.

Dyson, L. L. and Van Heerden, J.: A model for the identification of tropical weather systems over South Africa, Water SA, 28, 249-258, 2002.

Eglinton, G., Hamilton, R.J.: Leaf Epicuticular Waxes, Sci. J., 156, 1322-1335, 1967.

Ficken, K.J., Li, B., Swain, D.L., Eglinton, G.: An n-alkane proxy for the sedimentary input of submerged/floating freshwater aquatic macrophytes, Org. Geochem., 31, 745-749, 2000.

Ficken, K. J., Wooller, M. J., Swain, D. L., Street-Perrott, F. A., and Eglinton, G.: Reconstruction of a subalpine grass-dominated ecosystem, Lake Rutundu, Mount Kenya: a novel multi-proxy approach, Palaeogeography, Palaeoclimatology, Palaeoecology, 177, 137-149, 2002.

Finch, J.M., Hill, T.R.: A late Quaternary pollen sequence from Mfabeni Peatland, South Africa: Reconstructing forest history in Maputaland. Quaternary Res., 70, 442-450, 2008.

Fischer, H., Fundel, F., Ruth, U., Twarloh, B., Wegner, A., Udisti, R., Becagli, S., Castellano, E., Morganti, A., Severi, M., Wolff, E., Littot, G., Röthlisberger, R., Mulvaney, R., Hutterli, M.A., Kaufmann, P., Federer, U., Lambert, F., Bigler, M., Hansson, M., Jonsell, U., de Angelis, M., Boutron, C., Siggaard-Andersen, M.-L., Steffensen, J.P., Barbante, C., Gaspari, V., Gabrielli, P., Wagenbach, D.: Reconstruction of millennial changes in dust emission, transport and regional sea ice coverage using the deep EPICA ice cores from the Atlantic and Indian Ocean sector of Antarctica, Earth Planet. Sci. Lett., 260, 340-354. 2007.

Gasse, F., Chalié, F., Vincens, A., Williams, M. A. J., and Williamson, D.: Climatic patterns in equatorial and southern Africa from 30,000 to 10,000 years ago reconstructed from terrestrial and near-shore proxy data, Quaternary Science Reviews, 27, 2316-2340, 2008.

Gat, J.R., Mook, W.G., Meijer, H.A.: Environmental isotopes in the hydrological cycle, Water Resources Programme, 2001.

Gimeno, L., Drumond, A., Nieto, R., Trigo, R. M., and Stohl, A.: On the origin of continental precipitation, Geophysical Research Letters, 37, 2010.

Grab, S. W., and Simpson, A. J.: Climatic and environmental impacts of cold fronts over KwaZulu-Natal and the adjacent interior of southern Africa South African Journal of Science, 96, 602-608, 2000.

Grundling, P., Clulow, A.D., Price, J.S., Everson, C.S.: Quantifying the water balance of Mfabeni Mire (iSimangaliso Wetland Park, South Africa) to understand its importance, functioning and vulnerability, Mires Peat, 16, 1-18, 2015.

Grundling, P., Grootjans, A.P., Price, J.S., Ellery, W.N., Development and persistence of an African mire: How the oldest South African fen has survived in a marginal climate, CATENA, 110, 176-183, 2013.

Hart, N. C. G., Washington, R., and Reason, C. J. C.: On the Likelihood of Tropical–Extratropical Cloud Bands in the South Indian Convergence Zone during ENSO Events, Journal of Climate, 31, 2797-2817, 2018.

Helliker, B. R. and Ehleringer, J. R.: Establishing a grassland signature in veins: 18O in the leaf water of C3 and C4 grasses, Proceedings of the National Academy of Sciences, 97, 7894-7898, 2000.

Hogg, A.G., Hua, Q., Blackwell, P.G., Niu, M., Buck, C.E., Guilderson, T.P., Heaton, T.J., Palmer, J.G., Reimer, P.J., Reimer, R.W., Turney, C.S.M., Zimmerman, S.R.H., SHCal13 Southern Hemisphere Calibration, 0–50,000 Years cal BP, Radiocarbon, 55, 1889-1903, 2016.

Holmgren, K., Lee-Thorp, J. A., Cooper, G. R. J., Lundblad, K., Partridge, T. C., Scott, L., Sithaldeen, R., Siep Talma, A., and Tyson, P. D.: Persistent millennial-scale climatic variability over the past 25,000 years in Southern Africa, Quaternary Science Reviews, 22, 2311-2326, 2003.

Hua, Q., Barbetti, M., Rakowski, A.Z.: Atmospheric Radiocarbon for the Period 1950–2010, Radiocarbon, 55, 2059-2072, 2016.

Hudson, D.A., Hewitson, B.C.: The atmospheric response to a reduction in summer Antarctic sea-ice extent, Clim. Res., 16, 79-99. 2001

Huffman, T.N.: Intensive El Niño and the Iron Age of South-eastern Africa. J. Archaeol. Sci., 37, 2572-2586, 2010.

Humphries, M.S., Benitez-Nelson, C.R., Bizimis, M., Finch, J.M.: An aeolian sediment reconstruction of regional wind intensity and links to larger scale climate variability since the last deglaciation from the east coast of southern Africa. Global Planet. Change, 156, 59-67, 2017.

Humphries, M.S., Green, A.N., Finch, J.M.: Evidence of El Niño driven desiccation cycles in a shallow estuarine lake: The evolution and fate of Africa's largest estuarine system, Lake St Lucia. Global Planet. Change, 147, 97-105, 2016.

IPCC: Climate Change 2013: The Physical Science Basis. Contribution of Working Group I of the Fifth Assessment Report of the Intergovernmental Panel on Climate Change. , Cambridge University Press, 2013.

Kahmen, A., Schefuß, E., Sachse, D.: Leaf water deuterium enrichment shapes leaf wax n-alkane δD values of angiosperm plants I: Experimental evidence and mechanistic insights, Geochim. et Cosmochim. Ac., 111, 39-49, 2013.

Lamy, F., Hebbeln, D., Röhl, U., Wefer, G., Holocene rainfall variability in southern Chile: a marine record of latitudinal shifts of the Southern Westerlies, Earth Planet. Sci. Lett., 185, 369-382, 2001.

Lamy, F., Kilian, R., Arz, H.W., Francois, J.-P., Kaiser, J., Prange, M., Steinke, T.: Holocene changes in the position and intensity of the southern westerly wind belt, Nat. Geosci., 3, 695-699. 2010.

Laskar, J., Fienga, A., Gastineau, M., Manche, H.: La2010: a new orbital solution for the long-term motion, Astron. Astrophys., 532, 2011.

Lindesay, J.A.: South African rainfall, the Southern Oscillation and a Southern Hemisphere semi-annual cycle, J. Climatol., 8, 17-30, 1988.

Macron, C., Pohl, B., Richard, Y., and Bessafi, M.: How do Tropical Temperate Troughs Form and Develop over Southern Africa?, Journal of Climate, 27, 1633-1647, 2014.

Mason, S.J., Jury, M.R., Climatic variability and change over southern Africa: a reflection on underlying processes, Prog. Phys. Geog., 21, 23-50. 1997.

Meadows, M.E., Baxter, A.J.: Holocene vegetation history and palaeoenvironments at Klaarfontein Springs, Western Cape, South Africa, Holocene, 11, 699-706, 2001.

Meadows, M. E. and Sugden, J. M.: The late quaternary palaeoecology of a floristic kingdom: the southwestern Cape South Africa, Palaeogeography, Palaeoclimatology, Palaeoecology, 101, 271-281, 1993.

Monteith, J. L.: Reassessment of Maximum Growth Rates for C3 and C4 Crops, Experimental Agriculture, 14, 1-5, 1978.

Moy, C.M., Seltzer, G.O., Rodbell, D.T., Anderson, D.M.: Variability of El Nino/Southern Oscillation activity at millenial timescales during the Holocene epoch, Nature, 420, 162-165, 2002.

Munday, C. and Washington, R.: Circulation controls on southern African precipitation in coupled models: The role of the Angola Low. , Journal of Geophysical Research: Atmospheres,, 122, 861-877, 2017.

Neumann, F.H., Scott, L., Bousman, C.B., van As, L., A Holocene sequence of vegetation change at Lake Eteza, coastal KwaZulu-Natal, South Africa, Rev. Palaeobot. Palyno., 162, 39-53, 2010.

Nicholson, S.E., Flohn, H.: African environmental and climatic changes and the general atmospheric circulation in late pleistocene and holocene, Climatic Change, 2, 313-348, 1980.

Nicholson, S. E.: The intensity, location and structure of the tropical rainbelt over west Africa as factors in interannual variability, International Journal of Climatology, 28, 1775-1785, 2008.

Nkoana, R., Engelbrecht, F. A., and Marean, C. W.: Last Glacial Maximum simulations over southern Africa using a variable-resolution global model: synoptic-scale verification, 31st Conference of the South African Society for Atmospheric Science, Hennops River Valley, South Africa, 2015.

Osborne, C. P. and Sack, L.: Evolution of C4 plants: a new hypothesis for an interaction of CO2 and water relations mediated by plant hydraulics, Philosophical Transactions of the Royal Society B: Biological Sciences, 367, 583-600, 2012

Otto-Bliesner, B.L., Brady, E.C., Clauzet, G., Tomas, R., Levis, S., Kothavala, Z., Last Glacial Maximum and Holocene Climate in CCSM3, J. Clim., 19, 2526-2544, 2006.

Otto-Bliesner, B. L., Russell, J. M., Clark, P. U., Liu, Z., Overpeck, J. T., Konecky, B., deMenocal, P., Nicholson, S. E., He, F., and Lu, Z.: Coherent changes of southeastern equatorial and northern African rainfall during the last deglaciation, Science, 346, 1223-1227, 2014.

Partridge, T.C., Demenocal, P.B., Lorentz, S.A., Paiker, M.J., Vogel, J.C.: Orbital forcing of climate over South Africa: A 200,000-year rainfall record from the pretoria saltpan, Quaternary Sci.Rev., 16, 1125-1133, 1997.

Pinto, H., Sharwood, R. E., Tissue, D. T., and Ghannoum, O.: Photosynthesis of C3, C3-C4, and C4 grasses at glacial CO2, Journal of experimental botany, 65, 3669-3681, 2014.

Rácz, Z. and Smith, R. K.: The dynamics of heat lows, Quarterly Journal of the Royal Meteorological Society, 125, 225-252, 1999.

Reason, C.J.C., Mulenga, H.: Relationships between South African rainfall and SST anomalies in the Southwest Indian Ocean, Int. J. Climatol., 19, 1651-1673, 1999.

Risi, C., Bony, S., and Vimeux, F.: Influence of convective processes on the isotopic composition (δ18O and δD) of precipitation and water vapor in the tropics: 2. Physical interpretation of the amount effect, Journal of Geophysical Research: Atmospheres, 113, 2008.

Rodbell, D.T., Seltzer, G.O., Anderson, D.M., Abbott, M.B., Enfield, D.B., Newman, J.H.: A ~15,000-Year Record of El Niño-Driven Alluviation in Southwestern Ecuador, Sci. J., 283, 516-520, 1999.

Rojas, M., Moreno, P., Kageyama, M., Crucifix, M., Hewitt, C., Abe-Ouchi, A., Ohgaito, R., Brady, E.C., Hope, P.: The Southern Westerlies during the last glacial maximum in PMIP2 simulations. Clim. Dynam., 32, 525-548, 2009.

Sachse, D., Billault, I., Bowen, G.J., Chikaraishi, Y., Dawson, T.E., Feakins, S.J., Freeman, K.H., Magill, C.R., McInerney, F.A., van der Meer, M.T.J., Polissar, P., Robins, R.J., Sachs, J.P., Schmidt, H.-L., Sessions, A.L., White, J.W.C., West, J.B., Kahmen, A.: Molecular Paleohydrology: Interpreting the Hydrogen-Isotopic Composition of Lipid Biomarkers from Photosynthesizing Organisms. Annu. Rev. Earth Pl. Sc., 40, 221-249, 2012.

Sage, R. F.: The evolution of C4 photosynthesis, New Phytologist, 161, 341-370, 2004.

Sage, R. F., Wedin, D. A., and Li, M.: The Biogeography of C4 Photosynthesis: Patterns and Controlling Factors. In: C4 Plant Biology, Sage, R. F. and Monson, R. K. (Eds.), Academic Press, San Diego, 1999.

Sandweiss, D.H., Richardson, J.B., Reitz, E.J., Rollins, H.B., Maasch, K.A.: Geoarchaeological Evidence from Peru for a 5000 Years B.P, Onset of El Niño. Sci. J., 273, 1531-1533, 1996.

Schefuß, E., Kuhlmann, H., Mollenhauer, G., Prange, M., Pätzold, J., Forcing of wet phases in southeast Africa over the past 17,000 years, Nature, 480, 509, 2011.

Schefuß, E., Schouten, S., Schneider, R.R., Climatic controls on central African hydrology during the past 20,000 years, Nature, 437, 1003-1006, 2005.

Schmidt, F., Oberhänsli, H., Wilkes, H.: Biocoenosis response to hydrological variability in Southern Africa during the last 84kaBP: A study of lipid biomarkers and compound-specific stable carbon and hydrogen isotopes from the hypersaline Lake Tswaing, Global Planet. Change, 112, 92-104, 2014.

Scott, L.: Palynology of late Pleistocene hyrax middens, southwestern Cape Province, South Africa: A preliminary report, Historical Biology, 9, 71-81, 1994.

Scott, L., Holmgren, K., Talma, A.S., Woodborne, S., Vogel, J.C.: Age interpretation of the Wonderkrater spring sediments and vegetation change in the Savanna Biome, Limpopo province, South Africa : research letter, S. Afr. J. Sci., 99, 484-488, 2003.

Scott, L., Vegetation history and climate in the Savanna biome South Africa since 190,000 ka: a comparison of pollen data from the Tswaing Crater (the Pretoria Saltpan) and Wonderkrater. Quatern. Int., 57-58, 215-223, 1999.

Scott, L.: Fluctuations of vegetation and climate over the last 75 000 years in the Savanna Biome, South Africa: Tswaing Crater and Wonderkrater pollen sequences reviewed, Quaternary Sci. Rev., 145, 117-133, 2016.

Scott, L., Neumann, F.H., Brook, G.A., Bousman, C.B., Norström, E., Metwally, A.A.: Terrestrial fossil-pollen evidence of climate change during the last 26 thousand years in Southern Africa, Quaternary Sci. Rev., 32, 100-118, 2012.

Simon, M.H., Ziegler, M., Bosmans, J., Barker, S., Reason, C.J.C., Hall, I.R.: Eastern South African hydroclimate over the past 270,000 years, Nature, 5, 18153, 2015.

Sonzogni, C., Bard, E., and Rostek, F.: Tropical sea-surface temperatures during the Last Glacial Period: A view based on alkenones in Indian Ocean sediments, Quaternary Science Reviews, 17, 1185-1201, 1998.

Sprenger, M., Tetzlaff, D., Soulsby, C.: Soil water stable isotopes reveal evaporation dynamics at the soil–plant–atmosphere interface of the critical zone, Hydrol. Earth Syst. Sci., 21, 3839-3858, 2017.

Stock, W.D., Chuba, D.K., Verboom, G.A.: Distribution of South African C_3 and C_4 species of Cyperaceae in relation to climate and phylogeny, Austral Ecol., 29, 313-319, 2004.

Stone, A.E.C., Last Glacial Maximum conditions in southern Africa, Prog. Phys.l Geog., 38, 519-542, 2014.

Stuut, J.-B.W., Lamy, F.: Climate variability at the southern boundaries of the Namib (southwestern Africa) and Atacama (northern Chile) coastal deserts during the last 120,000 yr, Quaternary Res., 62, 301-309, 2004.

Stuut, J.-B. W., Crosta, X., van der Borg, K., and Schneider, R.: Relationship between Antarctic sea ice and southwest African climate during the late Quaternary, Geology, 32, 909-912, 2004.

Taylor, R., Kelbe, B., Haldorsen, S., Botha, G.A., Wejden, B., Været, L., Simonsen, M.B.: Groundwater-dependent ecology of the shoreline of the subtropical Lake St Lucia estuary, Environ. Geol., 49, 586-600, 2006.

Tierney, J.E., Russell, J.M., Huang, Y., Sinninghe Damste, J.S., Hopmans, E.C., Cohen, A.S.: Northern hemisphere controls on tropical southeast African climate during the past 60,000 years, Sci. J., 322, 252-255, 2008.

Tipple, B.J., Meyers, S.R., Pagani, M.: Carbon isotope ratio of Cenozoic CO2: A comparative evaluation of available geochemical proxies, Paleoceanography, 25, 1-11, 2010.

Todd, M. and Washington, R.: Circulation anomalies associated with tropical-temperate troughs in southern Africa and the south west Indian Ocean, Climate Dynamics, 15, 937-951, 1999.

Toggweiler, J.R., Russell, J.L., Carson, S.R.: Midlatitude westerlies, atmospheric CO2, and climate change during the ice ages, Paleoceanography, 21, 1-15, 2006.

Tyson, P.D.: Atmospheric circulation changes and palaeoclimates of southern Africa, S. Afr. J. Sci., 95, 194-201, 1999.

Tyson, P.D.: Climatic Change and Variability in Southern Africa, Oxford University Press, Cape Town, 1986.

Tyson, P. D. and Preston-Whyte, R. A.: The Weather and Climate of Southern Africa, Oxford University Press, Southern Africa, Cape Town, 2000.

van Zinderen Bakker, E. M.: The evolution of Late Quaternary palaeoclimates of southern Africa, Palaeoecology of Africa, 9, 160-202, 1976.

Venter, C.E.: The Vegetation Ecology of Mfabeni Peat Swamp, St Lucia, KwaZulu-Natal, University of Pretoria, Pretoria, 2003.

Vigaud, N., Richard, Y., Rouault, M., and Fauchereau, N.: Moisture transport between the South Atlantic Ocean and southern Africa: relationships with summer rainfall and associated dynamics, Climate Dynamics, 32, 113-123, 2009.

Vogel, J.C., Fuls, A., Ellis, R.P.: The geographical distribution of kranz grasses in south africa, S. Afr. J. Sci., 74, 209-215, 1978.

Vogts, A., Badewien, T., Rullkötter, J., Schefuß, E.: Near-constant apparent hydrogen isotope fractionation between leaf wax n-alkanes and precipitation in tropical regions: Evidence from a marine sediment transect off SW Africa, Org. Geochem., 96, 18-27, 2016.

Waelbroeck, C., Labeyrie, L., Michel, E., Duplessy, J.C., McManus, J.F., Lambeck, K., Balbon, E., Labracherie, M.: Sea-level and deep water temperature changes derived from benthic foraminifera isotopic records, Quaternary Sci. Rev., 21, 295-305, 2002.

Walker, N.D.: Links between South African summer rainfall and temperature variability of the Agulhas and Benguela Current systems, J. Geophys. Res-Occeans, 95, 3297-3319, 1990.

World Weather Online: https://www.worldweatheronline.com/saint-lucia-estuary-weather-averages/kwazulu-natal/za.aspx, last access: 9 May 2018.

Wündsch, M., Haberzettl, T., Cawthra, H.C., Kirsten, K.L., Quick, L.J., Zabel, M., Frenzel, P., Hahn, A., Baade, J., Daut, G., Kasper, T., Meadows, M.E., Mäusbacher, R.: Holocene environmental change along the southern Cape coast of South Africa – Insights from the Eilandvlei sediment record spanning the last 8.9 kyr, Global Planet. Change, 163, 51-66, 2018.

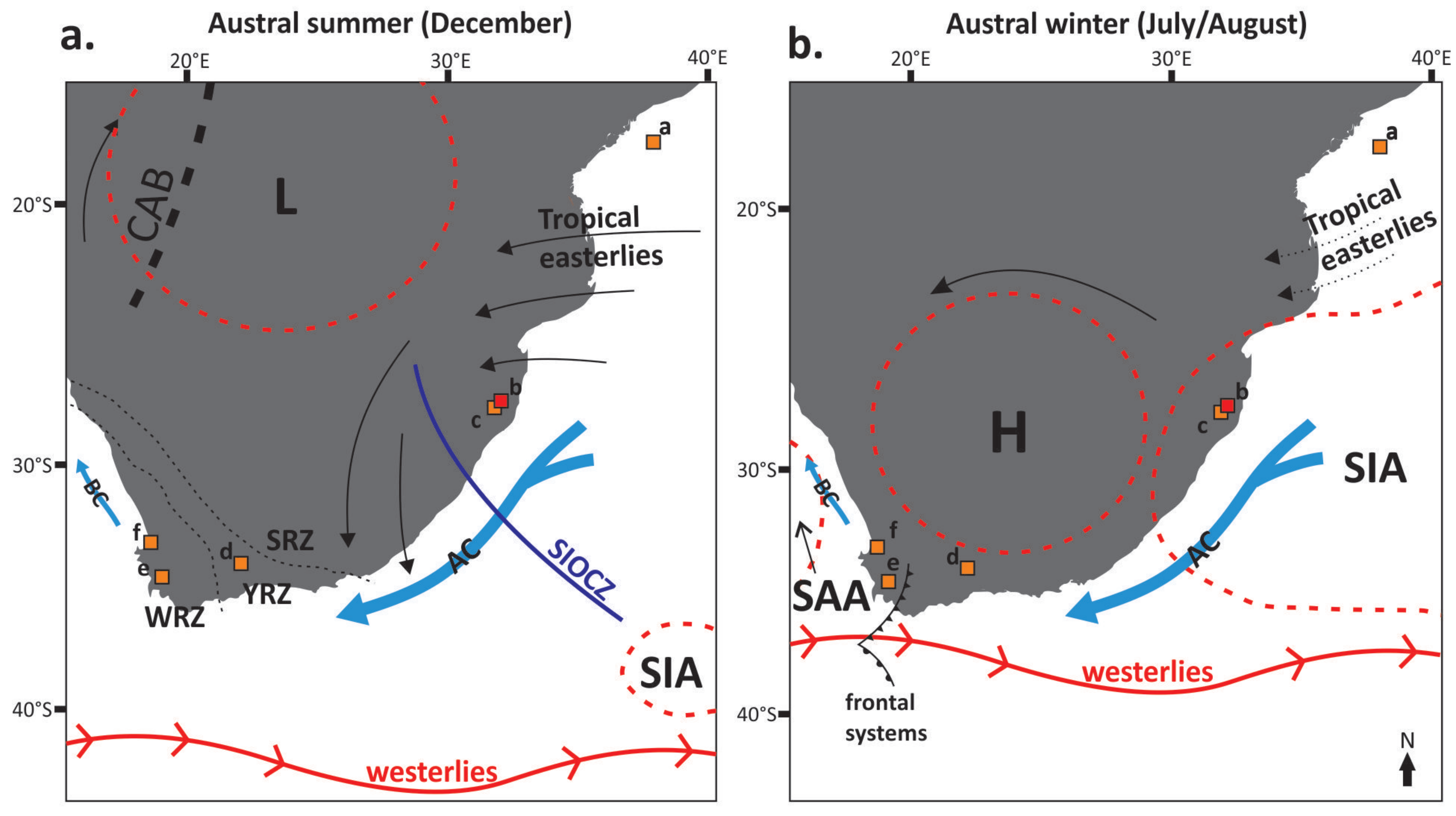
a.
Austral summer (December)
20°E
30°E
40°E
20°S
30°S
40°S
CAB
L
Tropical
easterlies
a
b
c
d
e
f
BC
SRZ
YRZ
WRZ
AC
SIOCZ
SIA
westerlies
b.
Austral winter (July/August)
20°E
30°E
40°E
20°S
30°S
40°S
a
Tropical
easterlies
H
b
c
SIA
BC
f
e
d
AC
SAA
westerlies
frontal
systems
N

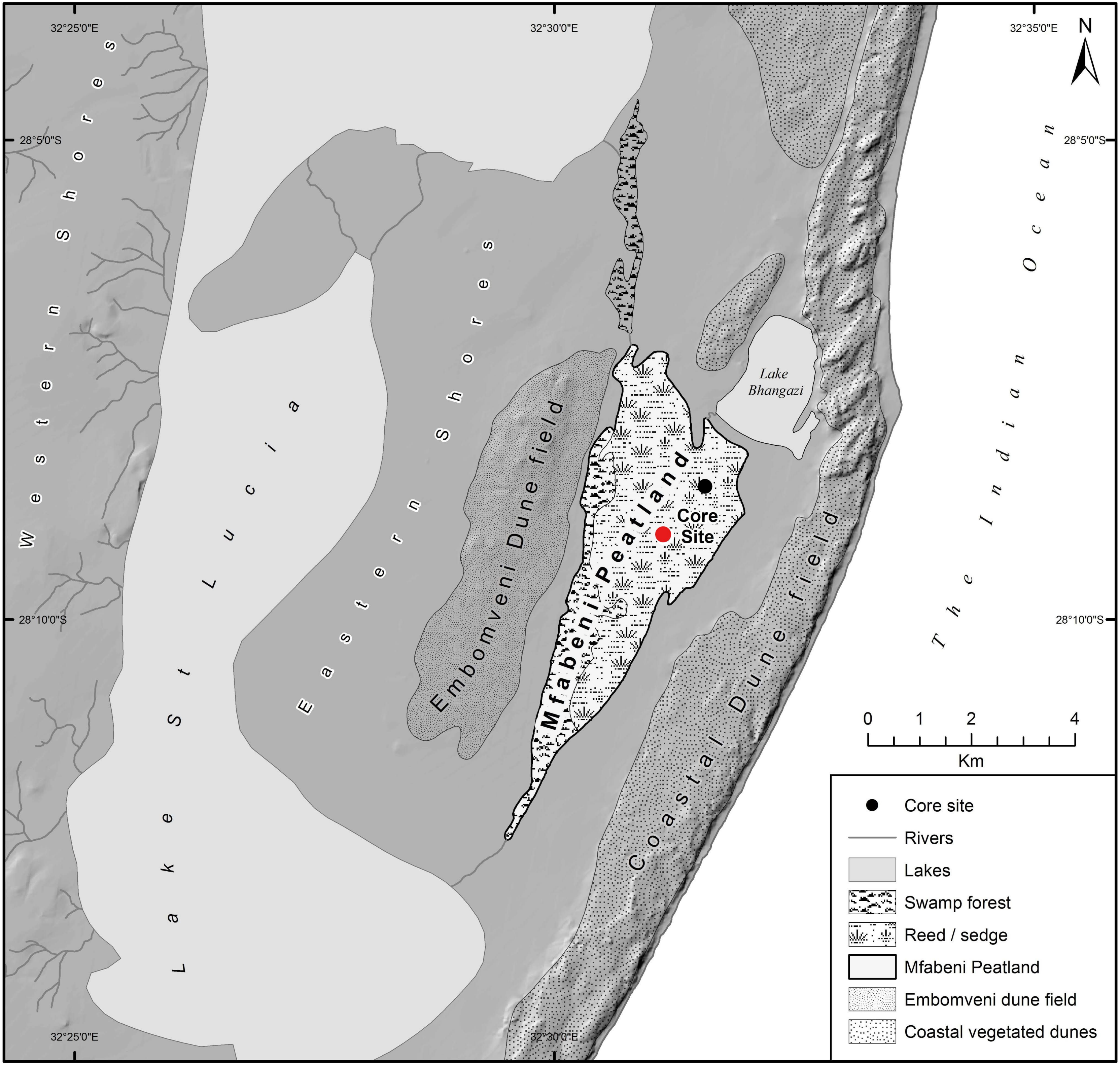

32°25'0"E
32°30'0"E
32°35'0"E
N
28°5'0"S
28°10'0"S
Western Shores
Eastern Shores
Lake St Lucia
Embomveni Dune field
Mfabeni Peatland
Core Site
Lake Bhangazi
Coastal Dune field
The Indian Ocean
0 1 2 4
Km
Core site
Rivers
Lakes
Swamp forest
Reed / sedge
Mfabeni Peatland
Embomveni dune field
Coastal vegetated dunes

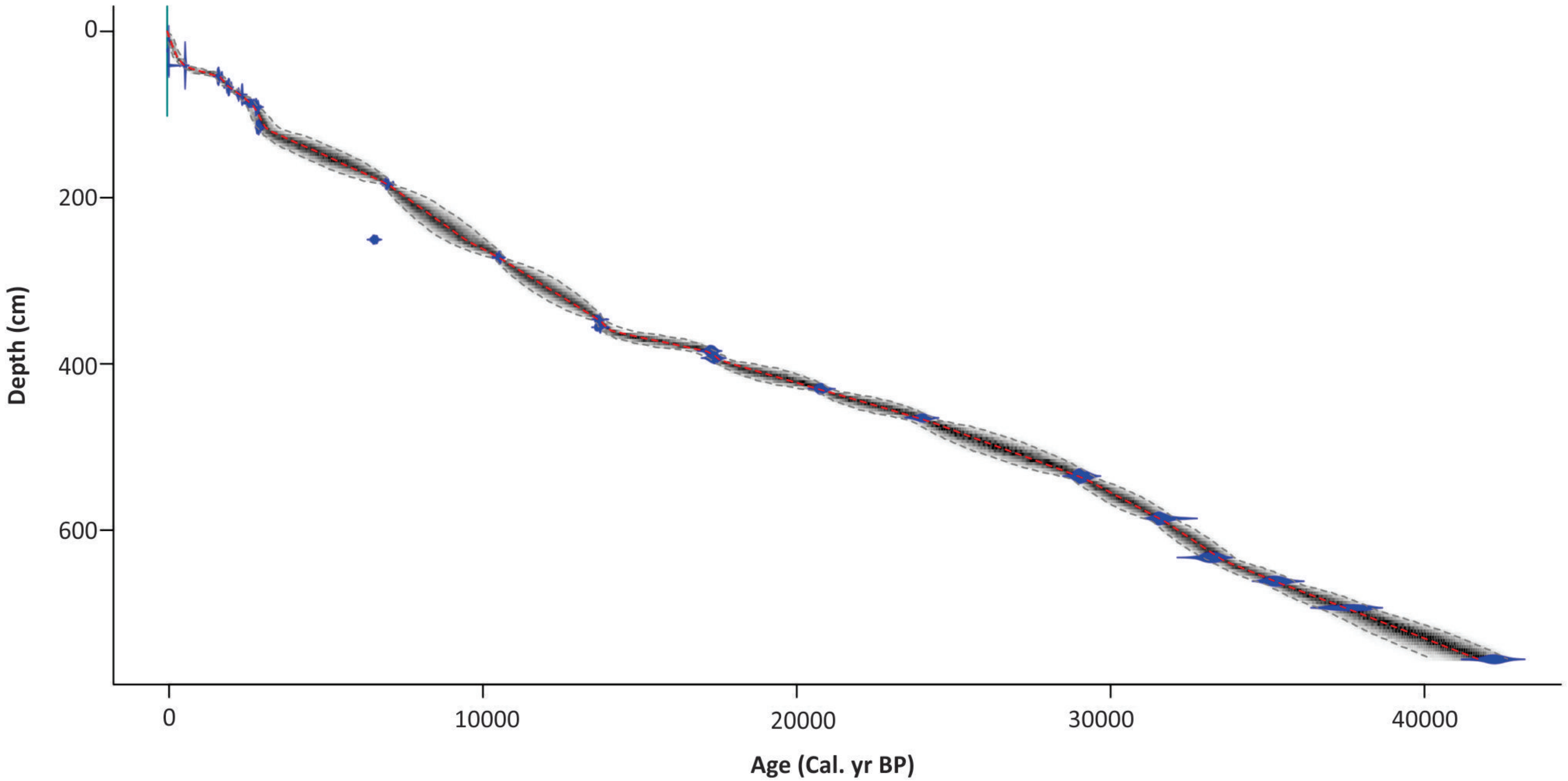

Depth (cm)
0
200
400
600
0
10000
20000
30000
40000
Age (Cal. yr BP)

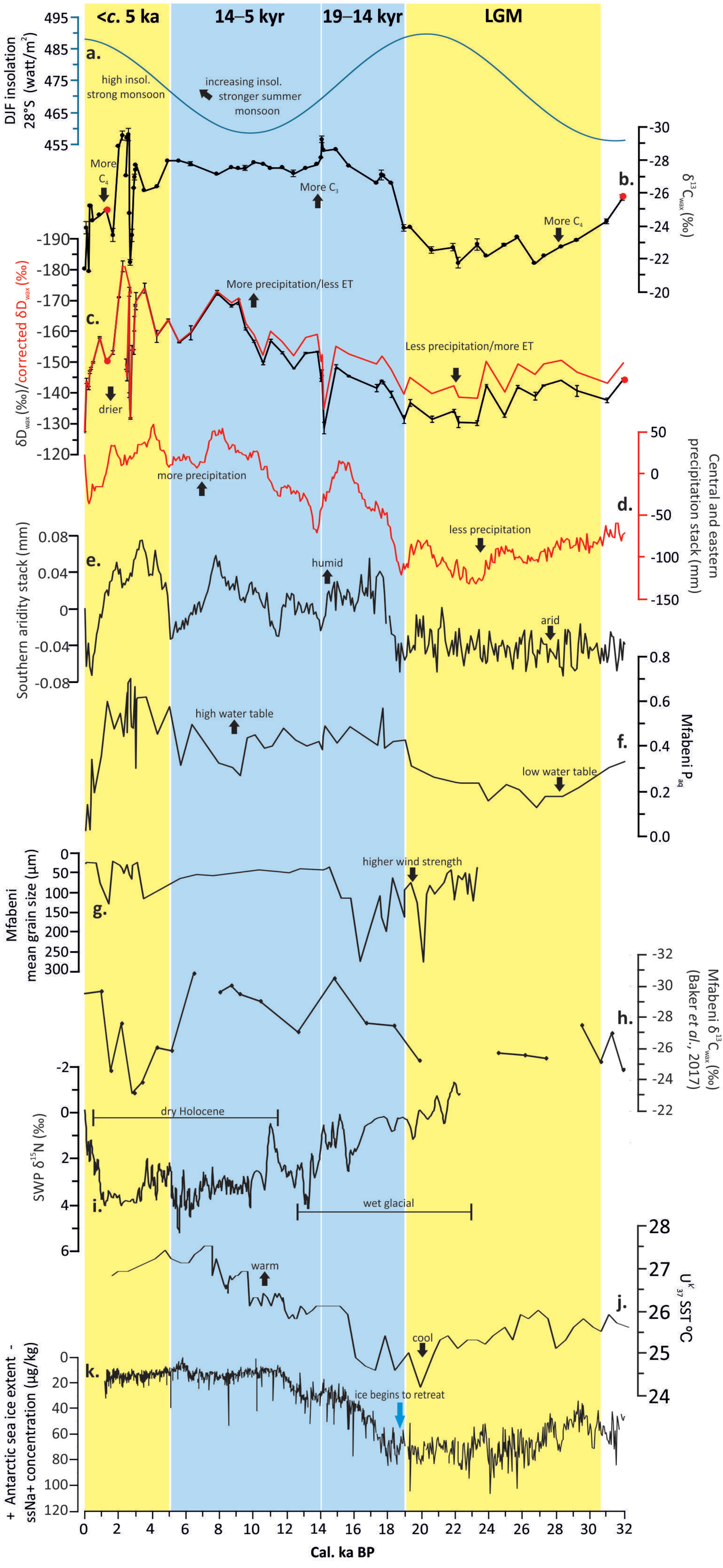

<c. 5 ka
14–5 kyr
19–14 kyr
LGM
DJF insolation 28°S (watt/m²)
a.
high insol. strong monsoon
increasing insol. stronger summer monsoon
b.
δ13Cwax (‰)
More C4
More C3
More C4
c.
δDwax (‰)/corrected δDwax (‰)
More precipitation/less ET
Less precipitation/more ET
drier
d.
Central and eastern precipitation stack (mm)
more precipitation
less precipitation
e.
Southern aridity stack (mm)
humid
arid
f.
Mfabeni Paq
high water table
low water table
g.
Mfabeni mean grain size (μm)
higher wind strength
h.
Mfabeni δ13Cwax (‰) (Baker et al., 2017)
SWP δ15N (‰)
dry Holocene
wet glacial
i.
j.
Uk'37 SST °C
warm
cool
k.
+ Antarctic sea ice extent - ssNa+ concentration (μg/kg)
ice begins to retreat
Cal. ka BP

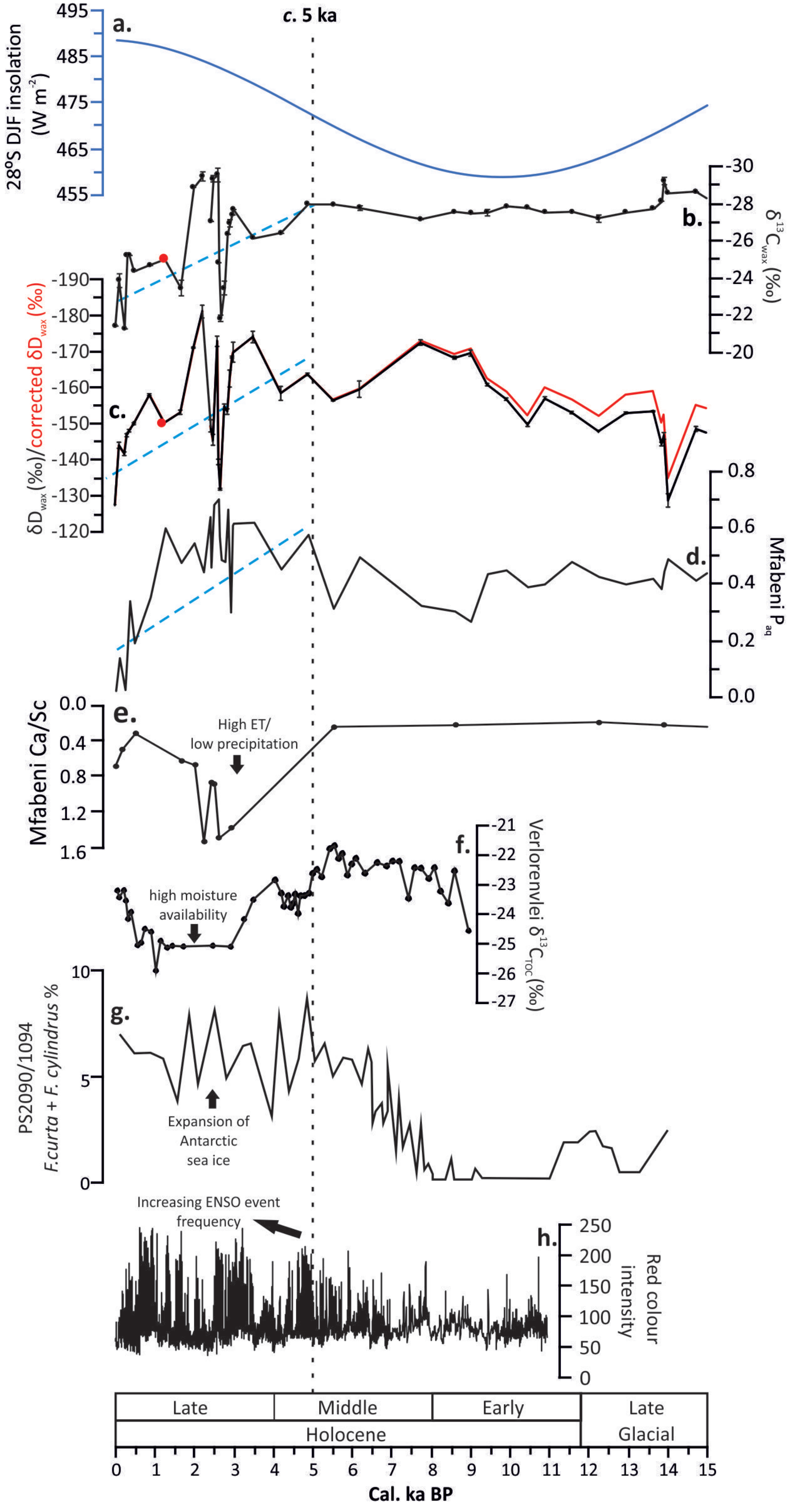

c. 5 ka
a.
28ºS DJF insolation (W m⁻²)
495
485
475
465
455
b.
δ13Cwax (‰)
-30
-28
-26
-24
-22
-20
c.
δDwax (‰)/corrected δDwax (‰)
-190
-180
-170
-160
-150
-140
-130
-120
d.
Mfabeni Paq
0.8
0.6
0.4
0.2
0.0
e.
Mfabeni Ca/Sc
0.0
0.4
0.8
1.2
1.6
High ET/
low precipitation
f.
Verlorenvlei δ13CTOC (‰)
-21
-22
-23
-24
-25
-26
-27
high moisture
availability
g.
PS2090/1094
F.curta + F. cylindrus %
10
5
0
Expansion of
Antarctic
sea ice
Increasing ENSO event
frequency
h.
Red colour intensity
250
200
150
100
50
0
Late
Middle
Early
Late
Holocene
Glacial
0
1
2
3
4
5
6
7
8
9
10
11
12
13
14
15
Cal. ka BP

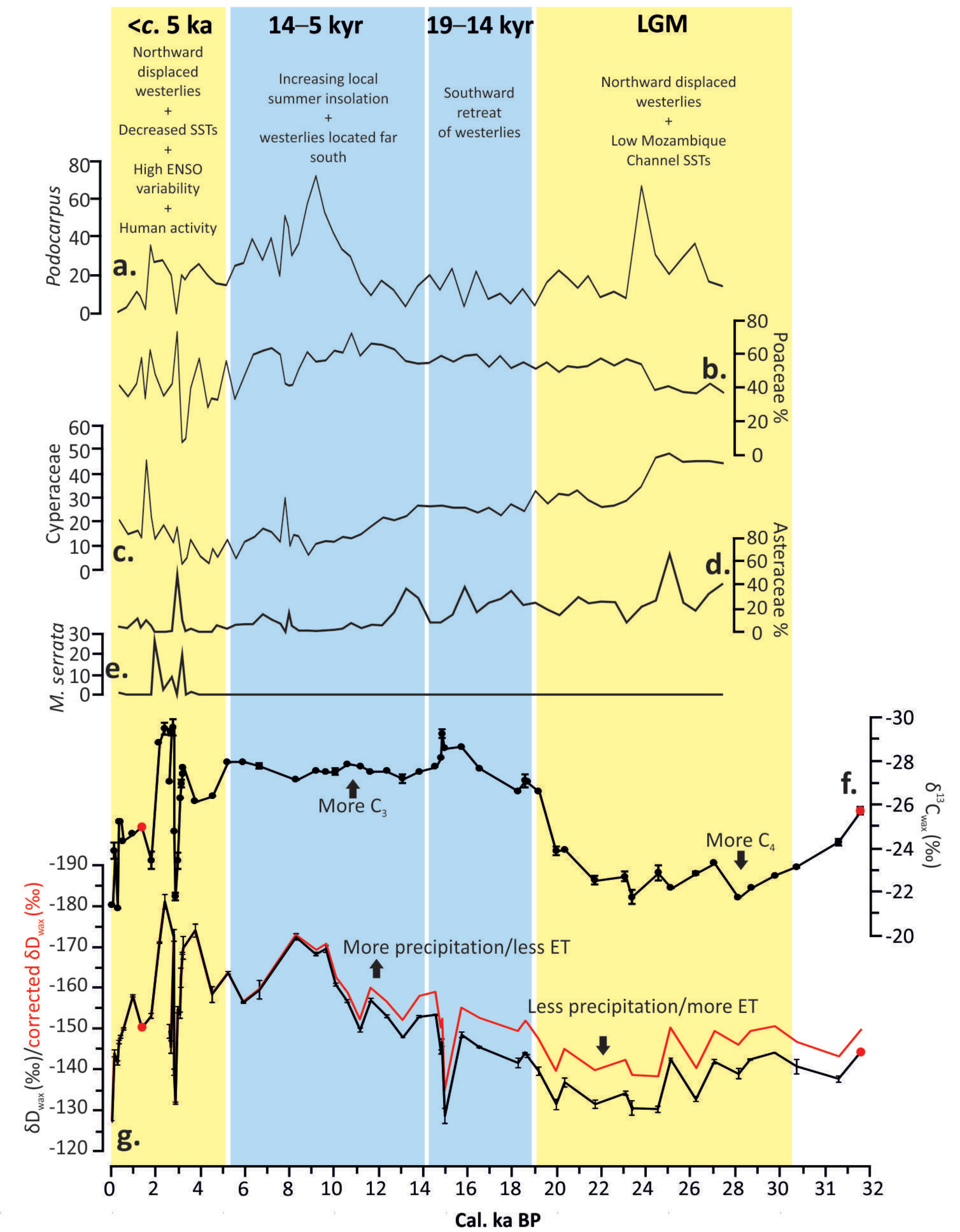

<c. 5 ka
14–5 kyr
19–14 kyr
LGM
Northward displaced westerlies + Decreased SSTs + High ENSO variability + Human activity
Increasing local summer insolation + westerlies located far south
Southward retreat of westerlies
Northward displaced westerlies + Low Mozambique Channel SSTs
a.
Podocarpus
b.
Poaceae %
c.
Cyperaceae
d.
Asteraceae %
e.
M. serrata
f.
More C3
More C4
δ13Cwax (‰)
g.
More precipitation/less ET
Less precipitation/more ET
δDwax (‰)/corrected δDwax (‰)
Cal. ka BP